Available online at www.sciencedirect.com
ScienceDirect
Comput. Methods Appl. Mech. Engrg. 373 (2021) 113448
Computer methods in applied mechanics and engineering
www.elsevier.com/locate/cma

Consistent weak forms for meshfree methods: Full realization of h-refinement, p-refinement, and a-refinement in strong-type essential boundary condition enforcement

Michael Hillman*, Kuan-Chung Lin

Department of Civil and Environmental Engineering, The Pennsylvania State University, University Park, PA 16802, USA

Received 14 May 2020; received in revised form 14 September 2020; accepted 15 September 2020
Available online xxxx

Graphical Abstract

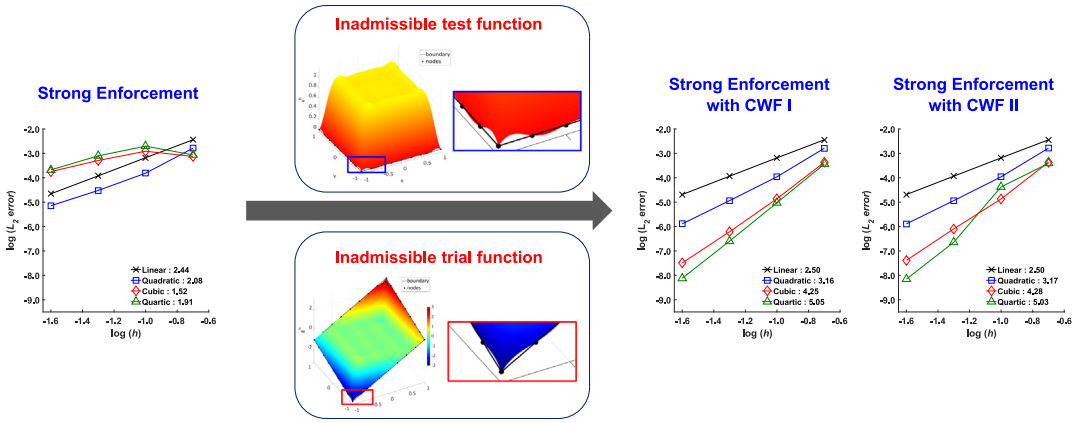

Abstract

Enforcement of essential boundary conditions in many Galerkin meshfree methods is non-trivial due to the fact that field variables are not guaranteed to coincide with their coefficients at nodal locations. A common approach to overcome this issue is to strongly enforce the boundary conditions at these points by employing a technique to modify the approximation such that this is possible. However, with these methods, test and trial functions do not strictly satisfy the requirements of the conventional weak formulation of the problem, as the desired imposed values can actually deviate between nodes on the boundary. In this work, it is first shown that this inconsistency results in the loss of Galerkin orthogonality and the best approximation property, and correspondingly, failure to pass the patch test. It is also shown that this induces an $\mathcal{O}(h)$ error in the energy norm in the solution of second-order boundary value problems that is independent of the order of completeness in the approximation. As a result, this places a barrier on the global order of accuracy of Galerkin meshfree solutions to that of linear consistency. That

* Correspondence to: 224A Sackett Building, The Pennsylvania State University, University Park, PA 16802, USA
E-mail address: mhillman@psu.edu (M. Hillman).

https://doi.org/10.1016/j.cma.2020.113448
0045-7825/© 2020 Elsevier B.V. All rights reserved.

is, with these methods, it is not possible to attain the higher order accuracy offered by meshfree approximations in the solution of boundary-value problems. To remedy this deficiency, two new weak forms are introduced that relax the requirements on the test and trial functions in the traditional weak formulation. These are employed in conjunction with strong enforcement of essential boundary conditions at nodes, and several benchmark problems are solved to demonstrate that optimal accuracy and convergence rates associated with the order of approximation can be restored using the proposed method. In other words, this approach allows p-refinement, and h-refinement with pth order rates with strong enforcement of boundary conditions beyond linear ($p > 1$) for the first time. In addition, a new concept termed a-refinement is introduced, where improved accuracy is obtained by increasing the kernel measure in meshfree approximations, previously unavailable.
© 2020 Elsevier B.V. All rights reserved.

Keywords: Meshfree methods; Essential boundary conditions; Refinement; Transformation method

1. Introduction

Galerkin meshfree methods [1] are a unique class of numerical approaches based on a purely point-based discretization. They offer advantages in classes of problems where mesh-based finite elements encounter difficulty, such as those involving extreme-deformation, multi-body evolving contact, fragmentation, among others; they also offer other attractive features like arbitrary smoothness or roughness uncoupled with the order of accuracy, ease of discretization, ease of adaptivity, and intrinsic enrichment [1–4]. However, their implementation is less trivial than the finite element method. For instance, careful attention needs to be paid to numerical quadrature, and enforcement of essential boundary conditions (cf. [1]). The focus of this work is the latter issue.

Enforcement of essential (or Dirichlet) boundary conditions is non-trivial in Galerkin meshfree methods since the nodal coefficients of shape functions do not coincide with their field variables at nodal locations in the general case. Colloquially, this is described as lacking the Kronecker delta property, or weak-Kronecker delta property (although an even weaker condition is sufficient to impose values at nodes on the boundary as will be discussed). Therefore, unlike the finite element method, essential boundary conditions cannot be directly enforced on the shape functions' coefficients. Several techniques have been proposed to overcome this difficulty.

In general, these methods can be classified into two categories: (1) strong enforcement of essential boundary conditions at nodal locations [5–9], and (2) weak enforcement of boundary conditions, such as the Lagrange multiplier method [10], the penalty method [7] and Nitsche's method [11,12]. In the first category, the idea is to modify the approximations such that nodal coefficients correspond to field variables on the essential boundary. For the second, these methods allow test and trial functions which do not need to satisfy any particular requirement related to the essential boundary, and instead impose boundary conditions weakly, i.e., in the sense of a distribution.

The first method proposed for enforcing essential boundary conditions in meshfree methods was the Lagrange multiplier approach used in the element free Galerkin (EFG) method [10]. While this circumvents the aforementioned difficulties in a relatively straight-forward manner, additional degrees of freedom are introduced, and the stiffness matrix is also positive semi-definite. The choice of the approximation for these multipliers is also subject to the *Ladyzhenskaya-Babuška-Brezzi (LBB) stability condition*, which is an inf-sup condition necessary for well-posedness of the discrete problem [13,14]; an approximation to the multiplier that is not "well-balanced" with the discretization of the primary variable will not yield a stable solution. Shortly after, a modified variational principle [15] was proposed to overcome these shortcomings. In this method, the idea is to substitute the physical meaning of the Lagrange multiplier (the constraint "forces") in terms of the primary variable back into the weak form; thus, the problem does not involve any additional degrees of freedom. However, this method does not guarantee stability either as it is equivalent to using a penalty value of zero in Nitsche's method, while a minimum penalty value is necessary for stability [16].

The penalty method is also a straight-forward way to enforce essential boundary conditions, which augments the potential with a weak penalty on the constraint. However, the solution is strongly dependent on the value of the penalty parameter: lower values lead to large errors on the essential boundary, while large values lead to an ill-conditioned system matrix [12]. Nitsche's method can be viewed, in some sense, as a combination of the modified variational principle and the penalty method. The solution error is much less sensitive to the value of the penalty parameter than the penalty method, as the penalty parameter plays an alternate role of ensuring solution stability rather than enforcing boundary conditions. Nevertheless, an extremely large or small parameter also leads

to the same issues as the penalty method [12]. A reliable way to select the parameter is based on an eigenvalue problem related to the discretization [16]. However, an important corollary is that the parameter depends on the discretization, and for meshfree methods that have a variety of free parameters, this entails the distribution of points, order of approximation, kernel measure, kernel function, etc. In the authors' experience, it is difficult to choose a suitable penalty parameter (to maintain desired convergence rates) *a priori* for accuracy higher than linear. More details on the effect and choice of the penalty value for these methods can be found in [12,16].

So far, the methods discussed are all in the class of weak enforcement of essential boundary conditions. Strong methods have been developed as well, which modify the approximation such that their enforcement is similar to the finite element method. The *transformation method* also known as the *collocation method* was first introduced in [5]. This method constructs the relationship between nodal coefficients and their field values in order to achieve the Kronecker delta property in the approximation. This however requires the inverse of a system-size matrix to solve the problem at hand. This technique was independently derived and discussed by several researchers later [6–9]. To avoid inverting a system-size matrix, a technique has been introduced to greatly reduce the size of the matrix involved in this method that needs to be inverted [7,17], which has been termed the *mixed transformation method*. It is worth mentioning the work in [17] offers convenient and simple implementations of these transformation methods with row-swap operations on the system matrix. Using these techniques is equivalent to employing Lagrange multipliers to enforce the essential boundary constraint point-wise at nodal locations [17].

Alternatively, approximations can also be constructed so that direct imposition of essential boundary conditions can be performed without inverting any matrices. These techniques are most convenient for explicit dynamic calculations for obvious reasons. Approaches include coupling of meshfree shape functions with finite elements near the essential boundary [18–20], employing singular kernel functions for nodes on the essential boundary of the domain [17], and constructing moving-least squares approximations with the interpolation property via primitive functions [21]. Forcing the correction function to be zero on the essential boundary has also been introduced [22], which yields the interpolation property (for a discussion on this aspect of meshfree approximations see [23]), but this technique is difficult to use in high dimensions and complex geometry. More recently a conforming kernel approximation has been introduced which possesses the weak Kronecker delta property, and can thus strictly satisfy the requirements on the test function (and for simple boundary conditions, the trial function) in the weak formulation [24]. Finally, outside of these two classes of methods, a novel way to impose boundary conditions using D'Alembert's principle was introduced in [25].

The most common method employed in the literature appears to be strong enforcement at nodal points. To the best of the authors' knowledge, there has been only one paper [21] examining the accuracy of higher-order meshfree approximations used with these strong-form type methods. There it was reported that while using quadratic basis *to approximate a function* can yield expected convergence rates, *employing it in the Galerkin equation* results in only first-order accuracy, a discrepancy which was attributed to a lack of verifying the desired conditions for test and trial functions in between the nodes.

In this paper, this assertion, and the effect of this discrepancy in the strong-type approach is closely examined, where it is shown that the requirements on test and trial functions in the weak form are indeed not verified between nodal locations. And, in fact, the difference between the desired values is of order h on the boundary (h is the nodal spacing), independent of the approximation order p. It is further shown that this discrepancy results in failure to pass the patch test, and loss of Galerkin orthogonality. Patch tests performed demonstrate that the L_2 norm of the error in the domain is restricted to order $\mathcal{O}(h^2)$ due to these inconsistencies, and order $\mathcal{O}(h)$ in the energy norm, regardless of the order of approximation employed.

Correspondingly, convergence rates much lower than expected are obtained for meshfree basis functions of order higher than linear ($p > 1$), and the rate of convergence is limited to that of employing approximations of linear consistency. To remedy these deficiencies, two weak forms are introduced that allow for larger spaces of test and trial functions. When employed with the strong-type methods, optimal convergence rates (for sufficiently regular solutions) are obtained. This technique thus allows, for the first time using strong methods, p-refinement, and h-refinement with pth order optimal rates beyond linear. Further, it is shown that the proposed method provides improved accuracy by increasing the kernel measure a in the meshfree approximation, previously unavailable, which is termed a-refinement.

The remainder of this paper is organized as follows. The reproducing kernel approximation is first introduced in Section 2 as a basis for examination of a typical meshfree method, and issues with strong essential boundary

condition enforcement are discussed. In Section 3, two weak forms are introduced which allow the enlargement of the approximation spaces to include meshfree approximations constructed under the strong-type enforcement techniques. Numerical procedures are described in Section 4, and numerical results are then given in Section 5 to demonstrate the effectiveness of the proposed methods. Section 6 provides concluding remarks.

2. Background

2.1. Reproducing kernel approximation

In this work, the reproducing kernel is chosen as a model approximation that does not strictly meet the requirements of the commonly used weak statement of a problem that includes Dirichlet boundary conditions.

Let a domain $\bar{\Omega} = \Omega \cup \partial\Omega$ be discretized by a set of Np nodes $S = \{\boldsymbol{x}_1, \ldots, \boldsymbol{x}_{Np} | \boldsymbol{x}_I \in \bar{\Omega}\}$ with corresponding node numbers $\eta = \{I | \boldsymbol{x}_I \in S\}$. The pth order discrete reproducing kernel (RK) approximation $u^h(\boldsymbol{x})$ of a function $u(\boldsymbol{x})$ is defined as [5,26]:

$$u^h(\boldsymbol{x}) = \sum_{I\in\eta} \Psi_I^{[p]}(\boldsymbol{x}) u_I \tag{1}$$

where $\{\Psi_I^{[p]}(\boldsymbol{x})\}_{I\in\eta}$ is the set of RK shape functions, and $\{u_I\}_{I\in\eta}$ are the associated coefficients.

The shape functions (1) are constructed by the product of a kernel function $\Phi_a(\boldsymbol{x} - \boldsymbol{x}_I)$ and a correction function $C^{[p]}(\boldsymbol{x}; \boldsymbol{x} - \boldsymbol{x}_I)$:

$$\Psi_I^{[p]}(\boldsymbol{x}) = \Phi_a(\boldsymbol{x} - \boldsymbol{x}_I) C^{[p]}(\boldsymbol{x}; \boldsymbol{x} - \boldsymbol{x}_I). \tag{2}$$

The correction function is composed of a linear combination of monomials up to order p, which allows the exact reproduction of these monomials and pth order accuracy in the approximation (1). In matrix form this function can be expressed as:

$$C^{[p]}(\boldsymbol{x}; \boldsymbol{x} - \boldsymbol{x}_I) = \boldsymbol{H}^{[p]}(\boldsymbol{x} - \boldsymbol{x}_I)^{\mathsf{T}} \boldsymbol{b}^{[p]}(\boldsymbol{x}) \tag{3}$$

where $\boldsymbol{H}^{[p]}(\boldsymbol{x})$ is a column vector of complete pth order monomials and $\boldsymbol{b}^{[p]}(\boldsymbol{x})$ is a column vector of coefficients. The coefficients are obtained by enforcing the following reproducing conditions:

$$\sum_{I\in\eta} \Psi_I^{[p]}(\boldsymbol{x}) \boldsymbol{H}^{[p]}(\boldsymbol{x}_I) = \boldsymbol{H}^{[p]}(\boldsymbol{x}), \tag{4}$$

or equivalently,

$$\sum_{I\in\eta} \Psi_I^{[p]}(\boldsymbol{x}) \boldsymbol{H}^{[p]}(\boldsymbol{x} - \boldsymbol{x}_I) = \boldsymbol{H}^{[p]}(\boldsymbol{0}). \tag{5}$$

Employing (2)–(5), the RK shape functions in (1) are constructed as:

$$\Psi_I^{[p]}(\boldsymbol{x}) = \boldsymbol{H}^{[p]}(\boldsymbol{0})^{\mathsf{T}} \{\boldsymbol{M}^{[p]}(\boldsymbol{x})\}^{-1} \boldsymbol{H}^{[p]}(\boldsymbol{x} - \boldsymbol{x}_I) \Phi_a(\boldsymbol{x} - \boldsymbol{x}_I) \tag{6}$$

where

$$\boldsymbol{M}^{[p]}(\boldsymbol{x}) = \sum_{I\in\eta} \boldsymbol{H}^{[p]}(\boldsymbol{x} - \boldsymbol{x}_I) \boldsymbol{H}^{[p]}(\boldsymbol{x} - \boldsymbol{x}_I)^{\mathsf{T}} \Phi_a(\boldsymbol{x} - \boldsymbol{x}_I) \tag{7}$$

and is called the moment matrix. Without modification, the approximation is in general non-interpolatory, that is, $u^h(\boldsymbol{x}_I) \neq u_I$. A simple demonstration of this property is given in Fig. 1.

2.2. Strong enforcement of essential boundary conditions at nodal locations

2.2.1. Model problem: Poisson's equation

Without loss of generality, in this work we consider the strong form ($\mathbb{S}$) of Poisson's equation as a model boundary value problem, which asks: given $s : \Omega \to \mathbb{R}$, $t : \partial\Omega_t \to \mathbb{R}$, and $g : \partial\Omega_g \to \mathbb{R}$, find $u : \bar{\Omega} \to \mathbb{R}$ such that the following conditions hold:

$$\nabla^2 u + s = 0 \quad \text{in } \Omega \tag{8a}$$

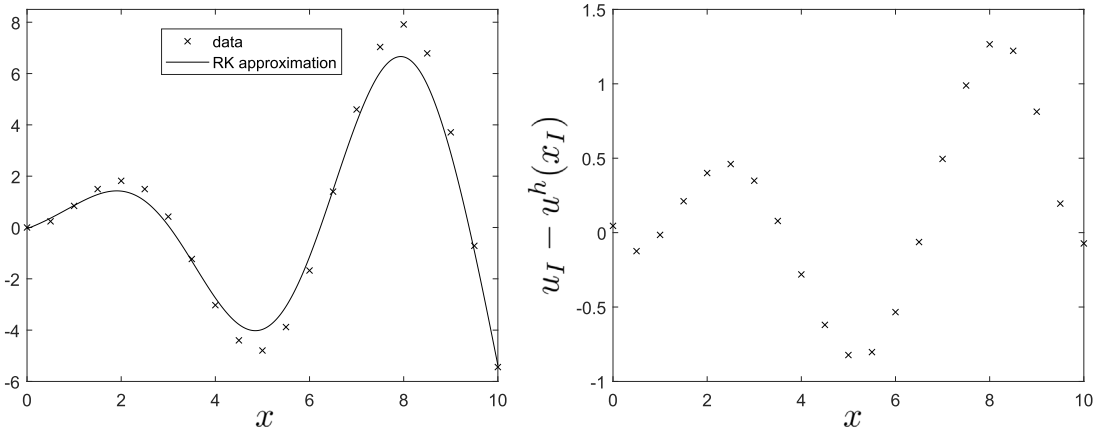

Fig. 1. Example of a meshfree approximation of data $u_I = x_I sin(x_I)$.

$$\nabla u \cdot \boldsymbol{n} = t \quad \text{on } \partial\Omega_t \tag{8b}$$

$$u = g \quad \text{on } \partial\Omega_g \tag{8c}$$

where $\nabla^2 \equiv \nabla \cdot \nabla$, and $\partial\Omega_t$ and $\partial\Omega_g$ denote the natural boundary and essential boundary, respectively, with $\partial\Omega_g \cap \partial\Omega_t = \emptyset$, $\partial\Omega = \overline{\partial\Omega_g \cup \partial\Omega_t}$, and $\bar{\Omega} = \Omega \cup \partial\Omega$.

2.2.2. Conventional Galerkin approximation

A weak form ($\mathbb{W}$) of Poisson's equation (8) can be constructed that seeks $u \in H^1_g$, $H^1_g = \{u | u \in H^1(\Omega), u = g \text{ on } \partial\Omega_g\}$ such that for all $v \in H^1_0$, $H^1_0 = \{v | v \in H^1(\Omega), v = 0 \text{ on } \partial\Omega_g\}$ the following equation holds:

$$a(v,u)_\Omega = (v,s)_\Omega + (v,t)_{\partial\Omega_t} \tag{9}$$

where

$$a(v,u)_\Omega = \int_\Omega \nabla v \cdot \nabla u \, \mathrm{d}\Omega, \tag{10a}$$

$$(v,s)_\Omega = \int_\Omega vs \, \mathrm{d}\Omega, \tag{10b}$$

$$(v,t)_{\partial\Omega_t} = \int_{\partial\Omega_t} vt \, \mathrm{d}\Gamma. \tag{10c}$$

With approximations v^h of test functions v and u^h of trial functions u, with $v^h = 0$ on $\partial\Omega_g$ and $u^h = g$ on $\partial\Omega_g$, a proper Galerkin approximation to (9) can be constructed which employs finite-dimensional subsets $\mathcal{S}_g \subset H^1_g$ and $\mathcal{S}_0 \subset H^1_0$, and seeks $u^h \in \mathcal{S}_g$ such that for all $v^h \in \mathcal{S}_0$ the following equation holds:

$$a(v^h,u^h)_\Omega = (v^h,s)_\Omega + (v^h,t)_{\partial\Omega_t}. \tag{11}$$

In approximations which possess the Kronecker delta property, and in particular the weak Kronecker delta property, a subset of H^1_0 is usually easily constructed. For instance, in linear finite elements, the boundary of the computational domain is defined by element edges where nodal values are linearly interpolated, so enforcement of a value of zero at nodes on the boundary ensures $v^h = 0$ on $\partial\Omega_g$. For any method with the weak Kronecker delta property and the partition of unity, the same argument follows. For construction of a subset of H^1_g, a common choice is to let the approximation interpolate values of g on the essential boundary, and $\mathcal{S}_g$ is also subset of H^1_g, or closely resembles a subset of H^1_g.

For meshfree methods which generally do not possess these properties, it is apparent from these discussions that the construction of subsets of H^1_0 and H^1_g is non-trivial.

2.3. Strong nodal imposition in meshfree methods

Strong imposition of essential boundary conditions at nodal locations is a popular choice in meshfree methods to (approximately, as will be shown) construct admissible test and trial functions for the conventional weak formulation (9). Essentially, these entail a modification of meshfree shape functions such that nodal degrees of freedom on the essential boundary coincide with their field variables. For this to be the case, the Kronecker delta property is not actually necessary [17,21], and instead the set of modified shape functions $\{\hat{\Psi}_I^{[p]}(\boldsymbol{x})\}_{I\in\eta}$ only need to verify the requirements:

$$\hat{\Psi}_J^{[p]}(\boldsymbol{x}_I) = 0 \quad \forall \quad I \in \eta_g, \quad J \in \eta \setminus \eta_g \tag{12}$$

and

$$\hat{\Psi}_I^{[p]}(\boldsymbol{x}_J) = \delta_{IJ} \quad \forall \quad I \in \eta_g, \quad J \in \eta_g \tag{13}$$

where δ_{IJ} is the Kronecker delta function, and $\eta\setminus\eta_g$ is the complement of the set of node numbers $\eta_g = \{I|\boldsymbol{x}_I \in S_g\}$ for nodes $S_g = \{\boldsymbol{x}_I|\boldsymbol{x}_I \in \partial\Omega_g\}$ located on the essential boundary. The above means that all "inside nodes" should not contribute to the approximation at "boundary nodes", while all "boundary nodes" need to verify the delta property at nodal locations on the boundary.

It is important to note that (12) and (13) only verify the prescribed conditions at nodal locations, but not in between nodes. Therefore one may enforce boundary conditions on nodal coefficients, as is done in the literature, but cannot ensure proper approximation spaces are constructed.

In contrast, the above properties are distinct from the weak Kronecker delta property, where only boundary shape functions contribute to the approximation on the *entire essential boundary*:

$$\hat{\Psi}_J^{[p]}(\boldsymbol{x}) = 0 \quad \forall \quad \boldsymbol{x} \in \partial\Omega_g, \quad J \in \eta \setminus \eta_g. \tag{14}$$

From the above, it is apparent that approximations with (14) will have little issue with constructing proper subsets (or very close approximations) necessary for the weak formulation (9). Meanwhile for meshfree approximations with only (12) and (13), and not (14), as is most common, constructing proper subsets is not possible.

2.3.1. Test function construction

Using these modified shape functions, in an attempt to construct a test space satisfying $\mathcal{S}_0 \subset H_0^1$, the following approximation is typically employed:

$$v^h(\boldsymbol{x}) = \sum_{I\in\eta\setminus\eta_g} \hat{\Psi}_I^{[p]}(\boldsymbol{x}) v_I \tag{15}$$

where $\{\hat{\Psi}_I^{[p]}(\boldsymbol{x})\}_{I\in\eta}$ is the set of modified shape functions with properties (12) and (13), and $\{v_I\}_{I\in\eta\setminus\eta_g}$ are coefficients of the test function.

Due to (12) and (13), the test functions verify $v^h(\boldsymbol{x}_I) = 0 \; \forall \; I \in \eta_g$. However, for these meshfree approximations, the value of $v^h(\boldsymbol{x})$ is in the general case, non-zero *between* nodes on the essential boundary and therefore violates the construction $\mathcal{S}_0 \subset H_0^1$.

To illustrate this, consider a domain $\bar{\Omega} = [-1, 1] \times [-1, 1]$ discretized uniformly in each direction by 9 nodes with $9 \times 9 = 81$ nodes total. A linear RK approximation ($p = 1$ in (15)) is employed using a cubic B-spline kernel function with a normalized support of 3. A test function with the arbitrary coefficients set to unity is constructed using the transformation method, with $\partial\Omega = \partial\Omega_g$. As seen in Fig. 2, the test functions are in fact non-zero between nodes along $\partial\Omega_g$ with the employment of (15). According to the norms computed in Table 1, the "error" (defined as non-zero values on the essential boundary) does converge at about a rate of one ($\mathcal{O}(h)$) in the $L^2(\partial\Omega_g)$ norm, yet the magnitude of the error (in $L^\infty(\partial\Omega_g)$) stays about the same regardless of the discretization. According to [27], the $L^2(\partial\Omega_g)$ error should be $\mathcal{O}(h^{3/2})$, however it seems to be $\mathcal{O}(h)$ when observed numerically, at least for meshfree approximations.

Next, the same setup is tested with $p = 2$ and $p = 3$, since a "linear" error occurs for the previous test, and linear basis was employed. The same norms are computed, shown in Tables 2 and 3, respectively for the two cases. Again an $\mathcal{O}(h)$ error is observed, and it is seen that this error is apparently independent of the order of approximation.

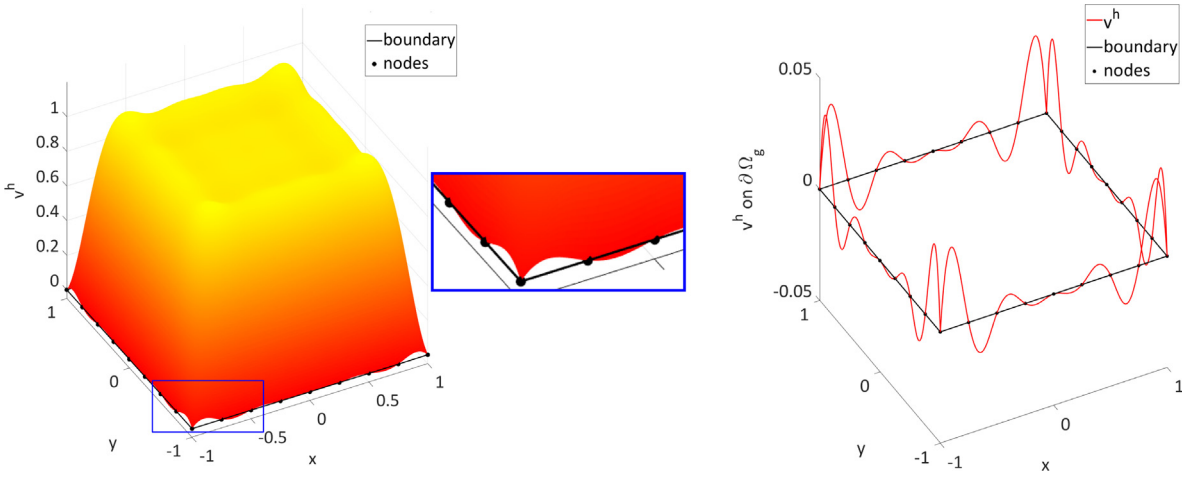

Fig. 2. Example of a test function in meshfree methods using the transformation method.

Table 1
Norms of error for boundary conditions imposed by test and trial functions, $p = 1$, varying h.

h	$L^2(\partial\Omega_g)$				$L^\infty(\partial\Omega_g)$	
	Test	Rate	Trial	Rate	Test	Trial
0.5000	0.01821	–	0.03615	–	0.03516	0.08443
0.2500	0.01014	0.84513	0.02137	0.75856	0.03645	0.10125
0.1250	0.00523	0.95507	0.01119	0.93372	0.03630	0.10495
0.0625	0.00262	0.99535	0.00573	0.96561	0.03628	0.10688

Table 2
Norms of error for boundary conditions imposed by test and trial functions, $p = 2$, varying h.

h	$L^2(\partial\Omega_g)$				$L^\infty(\partial\Omega_g)$	
	Test	Rate	Trial	Rate	Test	Trial
0.5000	0.01105	–	0.01935	–	0.02249	0.05458
0.2500	0.00352	1.65251	0.00640	1.59508	0.01476	0.03715
0.1250	0.00172	1.03368	0.00330	0.95787	0.01441	0.03723
0.0625	0.00086	1.00177	0.00176	0.90788	0.01440	0.03990

Table 3
Norms of error for boundary conditions imposed by test and trial functions, $p = 3$, varying h.

h	$L^2(\partial\Omega_g)$				$L^\infty(\partial\Omega_g)$	
	Test	Rate	Trial	Rate	Test	Trial
0.5000	0.00666	–	0.00975	–	0.01241	0.02231
0.2500	0.01016	−0.60978	0.01614	−0.72816	0.04419	0.09271
0.1250	0.00317	1.68073	0.00702	1.20050	0.02588	0.07773
0.0625	0.00163	0.95634	0.00353	0.99222	0.02653	0.07701

Later, it will be shown that this error can be directly related to the error in the energy norm of the problem—which will limit the rate of convergence for higher order ($p > 1$) approximations. This will then be confirmed numerically.

Finally, as a test, the kernel measure a is varied, with $p = 1$ and $h = 1/4$ fixed; the results are shown in Table 4. One can first observe that if $a \approx 1$ then the error (not shown to full significant digits) is machine precision; in this case the RK approximation closely resembles a bilinear finite element discretization. Then, as the kernel

Table 4
Norms of error for boundary conditions imposed by test and trial functions, $h = 1/4$, $p = 1$, varying a.

a	$L^2(\partial\Omega_g)$		$L^\infty(\partial\Omega_g)$	
	Test	Trial	Test	Trial
1.01	0.00000	0.00000	0.00000	0.00000
1.50	0.00118	0.00207	0.00592	0.01363
2.00	0.00483	0.00873	0.01821	0.04438
2.50	0.00863	0.01693	0.03007	0.08018
3.00	0.01014	0.02137	0.03645	0.10125
3.50	0.01085	0.02303	0.04106	0.11543
4.00	0.01207	0.02563	0.04533	0.13379

measure increases, the error on the boundary increases as well. It is generally expected that in the solution of partial differential equations (PDEs), that increasing the measure of an approximation will increase the accuracy of the solution; however this is not observed in practice, and an "optimal" value is observed in meshfree methods [26]. The increasing error on the boundary can explain that there exists two competing mechanisms: increasing error with increasing a due to failure to satisfy the requirements of test functions, and increasing the accuracy of the approximation with increasing a.

2.3.2. Trial function construction

Strong enforcement at boundary nodes $u^h(\boldsymbol{x}_I) = g(\boldsymbol{x}_I)$ is also typically introduced, and in an attempt to construct $\mathcal{S}_g \subset H^1_g$, the following approximation is employed:

$$u^h(\boldsymbol{x}) = \sum_{I\in\eta\setminus\eta_g} \hat{\Psi}^{[p]}_I(\boldsymbol{x})u_I + g^h(\boldsymbol{x}), \tag{16}$$

where

$$g^h(\boldsymbol{x}) = \sum_{I\in\eta_g} \hat{\Psi}^{[p]}_I(\boldsymbol{x})g_I, \tag{17}$$

the values $\{u_I\}_{\in\eta\setminus\eta_g}$ are the trial functions coefficients, and $g_I \equiv g(\boldsymbol{x}_I)$ is the prescribed value of $g(\boldsymbol{x})$ at an essential boundary node $\boldsymbol{x}_I \in \mathcal{S}_g$. Because of the properties (12) and (13), the trial functions verify $u^h(\boldsymbol{x}_I) = g(\boldsymbol{x}_I)\ \forall\ I \in \eta_g$.

While essential boundary conditions for trial functions are verified at nodal locations, the condition $u^h = g$ is again not enforced *between* the nodes. Fig. 3 depicts a linear function prescribed as $g(\boldsymbol{x}) = x+2y$ and approximated by (17) using the same discretization that was employed for the test function. Again it can be seen that along the boundary, the solution is collocated only at nodal points. As shown in Table 1, the $L^2(\partial\Omega_g)$ norm of the difference between g and g^h also converges at a rate of approximately one ($\mathcal{O}(h)$) just as the test function, while the magnitude of error (in $L^\infty(\partial\Omega_g)$) also stays roughly the same, despite refinement. It should be noted that even though linear bases are employed, the function is not exactly represented due to the influence of the interior nodes on the value of the meshfree approximation on the essential boundary between nodes. That is, it should be clear from Fig. 3 that the RK approximation under the transformation framework does not possess the weak Kronecker delta property.

Next, $p = 2$, and $p = 3$ are tested, with the same norms computed and shown in Tables 2 and 3, respectively. Again an $\mathcal{O}(h)$ error is observed, and it is seen that this error in representing the essential boundary conditions is also apparently independent of the order of approximation. The kernel measure a is again varied, with $p = 1$ and $h = 1/4$ fixed, and the results are shown in Table 4. Again for $a \approx 1$ the boundary conditions are represented quite well, as the RK approximation simply interpolates the boundary condition in the limit of $a \to 1$. Then, as the kernel measure increases, the error on the boundary increases as before.

In the next section, it will be shown that the errors on the boundary in the test and trial functions are directly related to the error in the solution of PDEs. That is, while $\mathcal{O}(h)$ in $L^2(\partial\Omega_g)$, the errors manifest as errors of $\mathcal{O}(h^2)$ in $L^2(\Omega)$ and $\mathcal{O}(h)$ in $H_1(\Omega)$, limiting the rate of convergence of the solution.

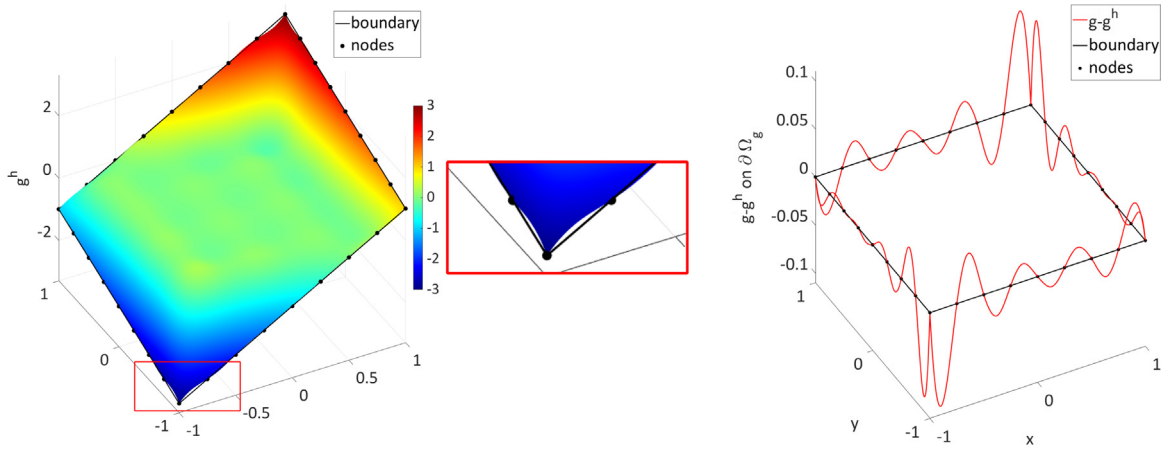

Fig. 3. Approximation $g^h(\boldsymbol{x})$ in meshfree methods using the transformation method.

2.3.3. Error assessment of inconsistencies

As a point of departure in considering the error induced by these inconsistencies, we first examine the weighted residual formulation, which is more a more general way to arrive at a weak formulation than a potential. The latter point of view will be revisited.

Integrating the product of an arbitrary weight function v and the residual of (8a) over Ω we have:

$$(v, \nabla^2 u + s)_\Omega = 0. \tag{18}$$

Integrating (18) by parts and employing divergence theorem one obtains

$$a(v,u)_\Omega = (v,s)_\Omega + (v, \boldsymbol{n}\cdot\nabla u)_{\partial\Omega}. \tag{19}$$

Per the usual procedures, employing (8b), $v = 0$ on $\partial\Omega_g$, and the boundary decomposition, we have the weak form $(\mathbb{W})$ in (9) which asks to find $u \in H^1_g$ such that for all $v \in H^1_0$ the following equation holds:

$$a(v,u)_\Omega = (v,s)_\Omega + (v,t)_{\partial\Omega_t}.$$

Provided u is sufficiently smooth, the above equation can be integrated by parts to obtain

$$(v, \nabla^2 u + s) + (v, t - \nabla u\cdot\boldsymbol{n})_{\partial\Omega_t} - (v, \nabla u\cdot\boldsymbol{n})_{\partial\Omega_g} = 0 \tag{20}$$

where

$$(v, \nabla u\cdot\boldsymbol{n})_{\partial\Omega_g} = \int_{\partial\Omega_g} v\nabla u\cdot\boldsymbol{n}\,\mathrm{d}\Gamma. \tag{21}$$

Employing the fact that $v = 0$ on $\partial\Omega_g$, $u = g$ on $\partial\Omega_g$, and the arbitrary nature of v one obtains the strong form (8), that is we have the following equivalence

$$(\mathbb{W}) \Leftrightarrow (\mathbb{S})$$

However, in meshfree methods it is difficult to achieve $v^h = 0$ on $\partial\Omega_g$ in the Galerkin discretization as discussed previously. And, in fact, as shown in [17], the transformation method is actually consistent with a weak formulation that only attests to strong enforcement of essential boundary conditions at nodal locations, rather than the entire essential boundary in the true strong form.

Either way, to demonstrate one significant consequence of employing (9), consider the following relation found by using Green's first identity and the conditions in (8):

$$\begin{aligned} a(v^h,u)_\Omega &= -(v^h,\nabla^2 u)_\Omega + (v^h, \boldsymbol{n}\cdot\nabla u)_{\partial\Omega} \\ &= (v^h,s)_\Omega + (v^h,t)_{\partial\Omega_t} + (v^h,\boldsymbol{n}\cdot\nabla u)_{\partial\Omega_g}. \end{aligned} \tag{22}$$

Subtracting (22) from (9) gives

$$a(v^h, u^h - u)_\Omega = (v^h, \boldsymbol{n} \cdot \nabla u^h)_{\partial\Omega_g} \tag{23}$$

which is the relation given in [27], and demonstrates that if $v^h \neq 0$ on $\partial\Omega_g$ Galerkin orthogonality is lost. It can be easily shown that using this relation, the best approximation property no longer holds, i.e., the minimum error in the norm induced by $a(\cdot,\cdot)$ is not obtained for the Galerkin solution. One immediate consequence is that the patch test will fail.

Now, as discussed in [27], the left hand side is bounded by $a(u^h - u, u^h - u)_\Omega^{1/2}$. Since the discrepancy on the boundary induced by the inadmissibility of test functions has been numerically observed as $\mathcal{O}(h)$, one should expect $\mathcal{O}(h)$ error in the energy norm of the problem, independent of the order of approximation. This will be confirmed numerically in the next Subsection.

Remark 1. To further elucidate the failure of the patch test, consider the viewpoint of variational consistency presented in [28]. Starting from (9), and following [28], it can be shown using (8) and (4), that the requirements for obtaining an exact solution $u^{[p]}$ of order p using the traditional weak formulation is

$$a\langle v^h, u^{[p]}\rangle_\Omega = -\langle v^h, \nabla^2 u^{[p]}\rangle_\Omega + \langle v^h, \boldsymbol{n} \cdot \nabla u^{[p]}\rangle_{\partial\Omega_t} \tag{24}$$

where $a\langle\cdot,\cdot\rangle$, $\langle\cdot,\cdot\rangle_\Omega$, and $\langle\cdot,\cdot\rangle_{\partial\Omega_t}$ denote the quadrature versions of $a(\cdot,\cdot)$, $(\cdot,\cdot)_\Omega$, and $(\cdot,\cdot)_{\partial\Omega_t}$, respectively. However, using integration by parts, with sufficiently high order (e.g. machine precision) quadrature it is obvious that

$$\begin{aligned} a\langle v^h, u^{[p]}\rangle_\Omega \approx -(v^h, \nabla^2 u^{[p]})_\Omega + (v^h, \boldsymbol{n} \cdot \nabla u^{[p]})_{\partial\Omega} \neq -(v^h, \nabla^2 u^{[p]})_\Omega + (v^h, \boldsymbol{n} \cdot \nabla u^{[p]})_{\partial\Omega_t} \approx -\langle v^h, \nabla^2 u^{[p]}\rangle_\Omega \\ + \langle v^h, \boldsymbol{n} \cdot \nabla u^{[p]}\rangle_{\partial\Omega_t} \end{aligned} \tag{25}$$

and a patch test will fail unless $v^h = 0$ on $\partial\Omega_g$. That is, no matter how high order the quadrature (or even with exact integration), one will not be able to pass the patch test. In addition, even if variationally consistent integration (VCI) is employed (which was developed to pass the patch test), one will still not be able to pass the patch test with strong-type essential boundary condition enforcement (unless $v^h = 0$ on $\partial\Omega_g$), since VCI-based methods are based on consistent weak forms (Nitsche's method, Lagrange multiplier, etc., see [28] for details) and one obtains:

$$a\langle v^h, u^{[p]}\rangle_\Omega = -\langle v^h, \nabla^2 u^{[p]}\rangle_\Omega + \langle v^h, \boldsymbol{n} \cdot \nabla u^{[p]}\rangle_{\partial\Omega} \neq -\langle v^h, \nabla^2 u^{[p]}\rangle_\Omega + \langle v^h, \boldsymbol{n} \cdot \nabla u^{[p]}\rangle_{\partial\Omega_t} \tag{26}$$

where $\langle\cdot,\cdot\rangle_{\partial\Omega}$ denotes the quadrature version of $(\cdot,\cdot)_{\partial\Omega}$. That is, these methods are incompatible with the inconsistent (traditional) weak form. On the other hand, as will be seen later in the text, the consistent weak forms proposed in Section 3 are in fact compatible with VCI methods.

2.3.4. Numerical assessment of the order of errors in boundary value problems

To examine the effect of these inconsistencies on the numerical solution to PDEs, and verify the assertions made in the previous section, a few patch tests are first performed, with the solution obtained using the transformation method.

Consider the Poisson problem (8) on the domain $\bar{\Omega} = [-1, 1] \times [-1, 1]$ with the pure essential boundary condition $\partial\Omega_g = \partial\Omega$. First, let the prescribed body force and boundary conditions be consistent with the linear solution $u = 0.1x + 0.3y$:

$$u = 0.1x + 0.3y \quad \text{on } \partial\Omega_g, \tag{27a}$$

$$s = 0 \quad \text{in } \Omega. \tag{27b}$$

Since the patch test in meshfree methods is intimately related with quadrature [28], the effect of the order of quadrature is first considered. That is, according to conventional wisdom, a failure of the patch test in meshfree methods is generally attributed to the lack of quadrature accuracy in the weak formulation. However, as has been discussed, no matter the accuracy of quadrature employed, one will not be able to pass the patch test with the weak formulation in conjunction with a strong-type boundary method. In addition, as discussed in Remark 1, the VCI technique used to patch past tests will not succeed.

To demonstrate this, the patch test is first performed with varying orders of quadrature denoted NQ. Gauss cells with $NQ \times NQ$ rules are employed that are coincident with the nodal spacing such that each cell is associated

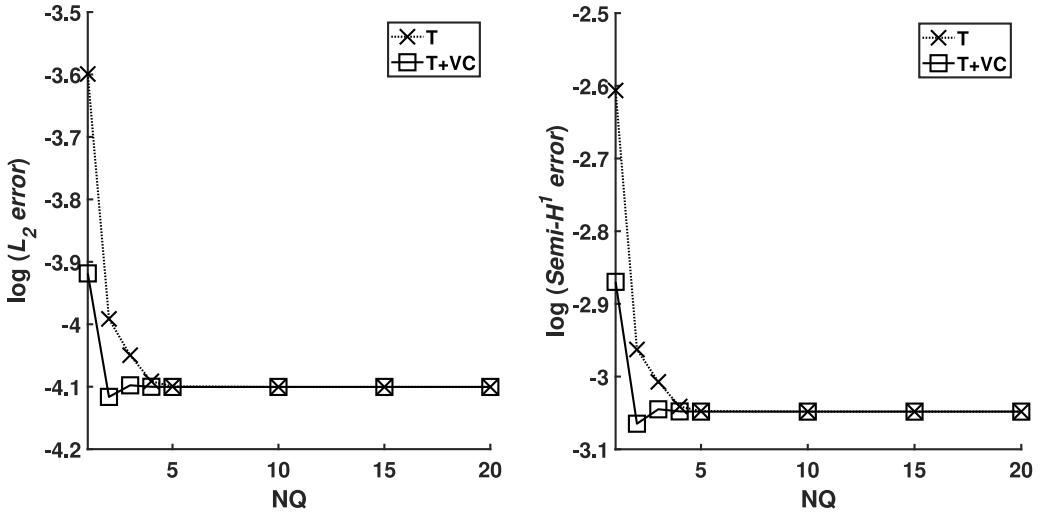

Fig. 4. Norms of error for the transformation method in a linear patch test in Poisson's problem with respect to number of quadrature points "NQ". "T" denotes transformation, "T+VC" denotes transformation using VCI.

with four nodes, with boundary Gauss points defined by the outer segments of cells intersecting $\partial\Omega$ for integration of boundary terms. Cubic B-spline kernels are employed for the RK approximation, with normalized supports of $p+1$. This integration scheme and choice of kernel functions will be employed throughout this manuscript unless otherwise stated.

Linear basis is used in the RK approximation so that the solution can be represented exactly. VCI is also employed to verify the relations stated in Remark 1. The domain is discretized uniformly with a nodal spacing of $h = 1/5$. As seen in Fig. 4, no matter the order of accuracy of quadrature, the patch test cannot be passed (error on the level of machine precision). Increasing the quadrature accuracy does not result in a better solution, and in fact, the solution error converges at $NQ = 5$. That is, increasing the order quadrature past this point has little effect on the solution. In addition, it can be seen that the VCI technique also does not pass the patch test with strong-type essential boundary condition enforcement.

As a result of this study, $NQ = 5$ will be employed for the following patch test studies in this Subsection, and any remaining error should be due to other *variational crimes*: the only inconsistency present in the formulation then is the inability to satisfy the requirements on test and trial functions in the weak form [27].

Standard convergence of the solution (with respect to h) is now tested, with the errors in the $L_2(\Omega)$ norm and $H^1(\Omega)$ semi-norm shown in Fig. 5. VCI is again employed to verify the relations stated in Remark 1. First, it can be seen that the patch tests are indeed not passed, which can be attributable to the errors in constructing the proper approximation spaces, since there are no other variational crimes committed (the quadrature error should be negligible according to Fig. 4). Also, with the addition of VCI, one is still not able to pass the patch test, and the error is generally unaffected.

Importantly, it is also seen that through refinement of the discretization (decreasing h), the order of error induced by the inconsistency in the boundary conditions on the test and trial functions manifest as $\mathcal{O}(h^2)$ and $\mathcal{O}(h)$, for the $L_2(\Omega)$ norm and $H^1(\Omega)$ semi-norm, respectively. That is, the errors reduce with refinement, at a rate consistent with employing linear basis. One may thus expect that these errors will have no influence on the convergence rates in the solution of PDEs with linear basis, but will have influence on solutions using higher order basis, which will be confirmed later.

Next, consider a quadratic patch test with quadratic basis with the same test of h-refinement. Here the following quadratic solution is considered: $u = 0.1x + 0.3y + 0.8x^2 + 1.2xy + 0.6y^2$. The following conditions result in this solution:

$$u = 0.1x + 0.3y + 0.8x^2 + 1.2xy + 0.6y^2 \quad \text{on } \partial\Omega_g, \tag{28a}$$

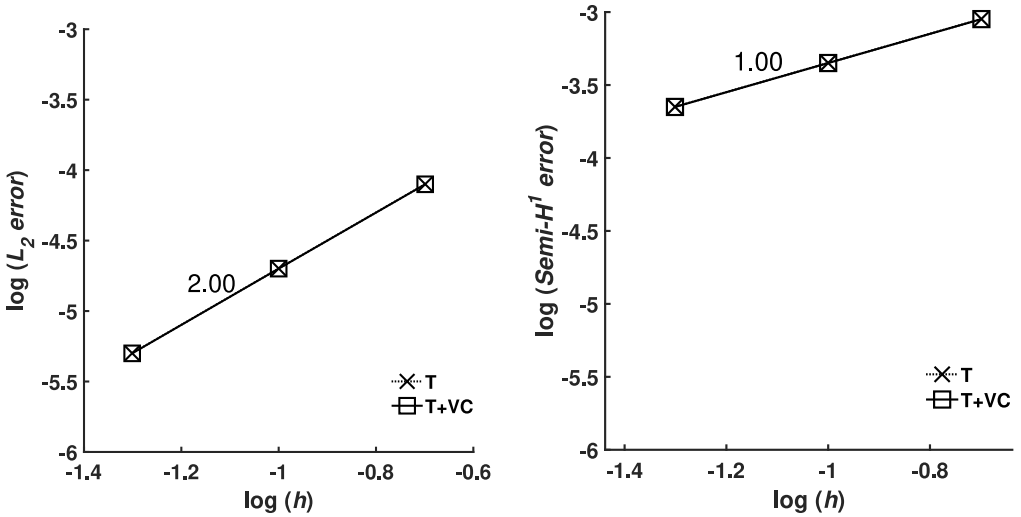

Fig. 5. Norms of error for the transformation method in a linear patch test in Poisson's problem, rate of convergence indicated. "T" denotes transformation, "T+VC" denotes transformation using VCI.

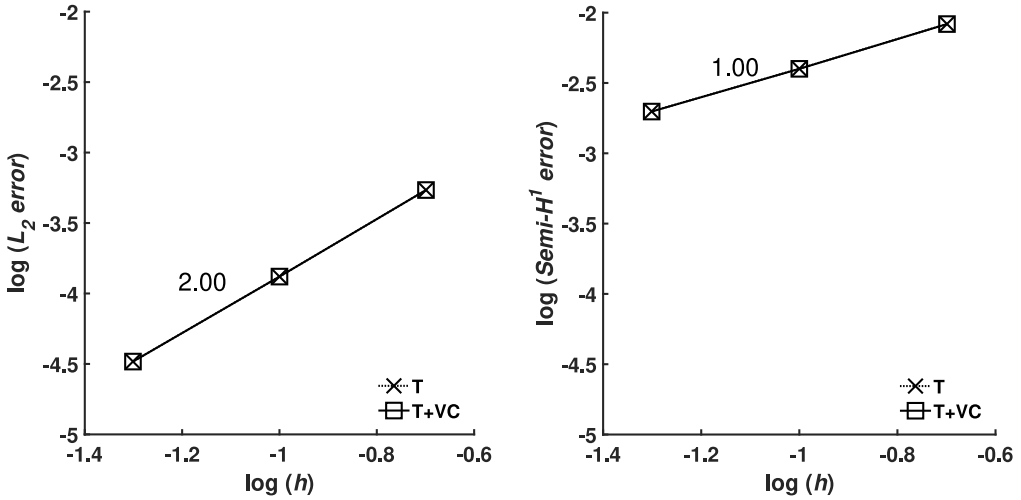

Fig. 6. Norms of error for the transformation method in a quadratic patch test in Poisson's problem, rate of convergence indicated. "T" denotes transformation, "T+VC" denotes transformation using VCI.

$$s = -2.8 \qquad \text{in } \Omega. \tag{28b}$$

The error in the $L_2(\Omega)$ norm and $H^1(\Omega)$ semi-norm are shown in Fig. 6. First, it can be seen that indeed no method can pass the patch test, even when VCI is employed. This is again attributable to the inconsistency of the weak formulation used in conjunction with the strong approach to boundary conditions.

It can also be seen that the inconsistent enforcement of boundary conditions results in errors $\mathcal{O}(h^2)$ and $\mathcal{O}(h)$ in the previously mentioned norms, respectively. That is, the errors again decrease at a rate consistent with "linear" accuracy, despite the fact that higher-order accurate basis functions are employed. One may then expect that these errors will limit the order of convergence in the solution of PDEs, which again, will be confirmed later.

To conclude, these results indicate that quadrature is not the only factor that influences the ability to pass the patch test, and in fact, using the strong-type enforcement of boundary conditions in conjunction with the conventional weak formulation precludes this. The failure of the patch test using VCI also indicates that the transformation method must be corrected in some way in order to use VCI effectively for these strong methods. Importantly, the inability

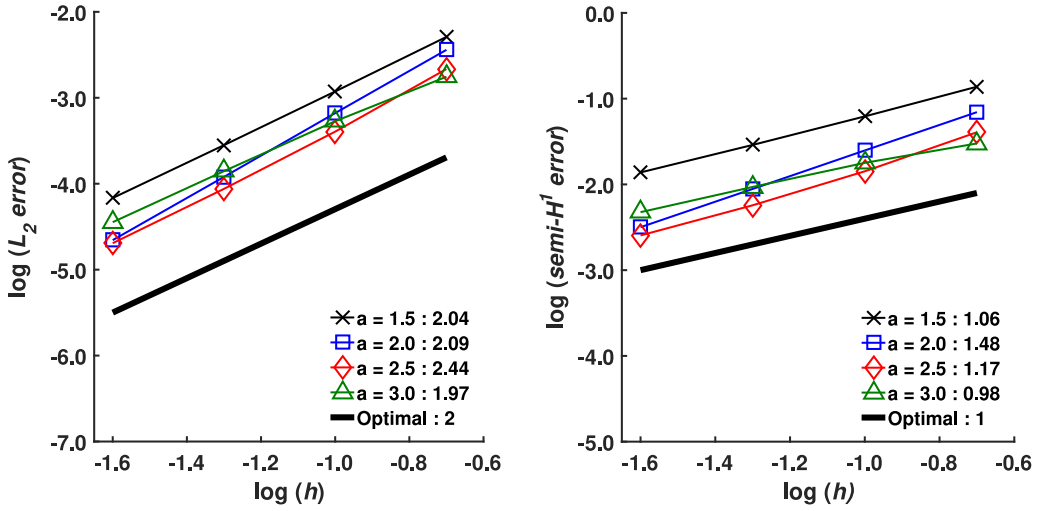

Fig. 7. Convergence of transformation method with linear basis with various kernel measures a: rates indicated in legend.

to construct proper approximation spaces also yields errors of linear order in the solution of PDEs, independent of the order of completeness employed.

To examine the possible, and now expected, effect on convergence rates, consider (8) with the source term and pure essential boundary $\partial\Omega_g = \partial\Omega$ with domain $\bar{\Omega} = [0, 1] \times [0, 1]$:

$$g(x, 0) = \sin(\pi x), \quad g(x, 1) = g(0, y) = g(1, y) = 0 \quad \text{on } \partial\Omega_g, \tag{29a}$$

$$s = 0 \quad \text{in } \Omega. \tag{29b}$$

The exact solution of this problem is high order [12]:

$$u = \{\cosh(\pi y) - \coth(\pi)\sinh(\pi y)\}\sin(\pi x). \tag{30}$$

Linear, quadratic, and cubic bases are employed with the transformation method, with uniform refinements of the domain. Various normalized support sizes (denoted "a" in the Figure legends) are employed, to examine the effect of varying the measure of $\Phi_a(\boldsymbol{x} - \boldsymbol{x}_I)$, as it is well known that linear basis degenerates to linear finite elements as the normalized measure a approaches unity. Thus, larger values of a are expected to show more pronounced error due to boundary condition enforcement, since finite elements have little to no difficulty in constructing proper approximation spaces, or at least ones which do not induce significant solution errors. In these convergence tests, 20×20 quadrature is employed to isolate the effects of the boundary condition enforcement completely (see Fig. 4).

Fig. 7 shows the convergence for linear basis in the $L_2(\Omega)$ norm and $H^1(\Omega)$ semi-norm; it can be seen that the optimal rates of two and one are essentially maintained, regardless of the kernel measure.

For quadratic basis, it can be seen in Fig. 8 that these same *linear* rates are also generally obtained, yet the optimal rates for quadratic basis *should be three and two* for the $L_2(\Omega)$ norm and $H^1(\Omega)$ semi-norm, respectively. Therefore optimal rates are not obtained in this case, and rather, the solution exhibits linear accuracy rather than quadratic.

For the case of cubic basis, shown in Fig. 9, it can again be seen that the rates obtained are far lower than expected; the *linear rates* of two and one are again obtained in most cases for the $L_2(\Omega)$ norm and $H^1(\Omega)$ semi-norm, respectively, when the optimal convergence rates associated with employing approximations with cubic completeness are four and three, respectively. Again, the solution exhibits linear accuracy, rather than cubic.

Higher order bases were also tested but are not shown here for conciseness of presenting the present study. The transformation method also provided only linear solution accuracy.

To conclude, the numerical results in this section indicate that the error due to the inability to satisfy the requirements of the conventional weak form (9) is characterized as $\mathcal{O}(h^2)$ error in the $L_2(\Omega)$ norm and $\mathcal{O}(h)$ error in the $H^1(\Omega)$ semi-norm, limiting the rate of convergence for bases higher than linear.

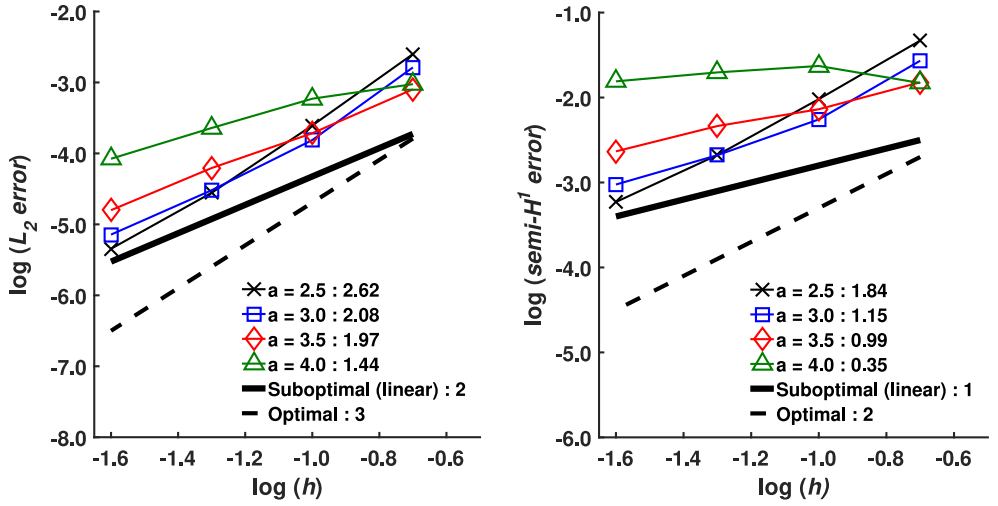

Fig. 8. Convergence of transformation method with quadratic basis with various kernel measures a: rates indicated in legend.

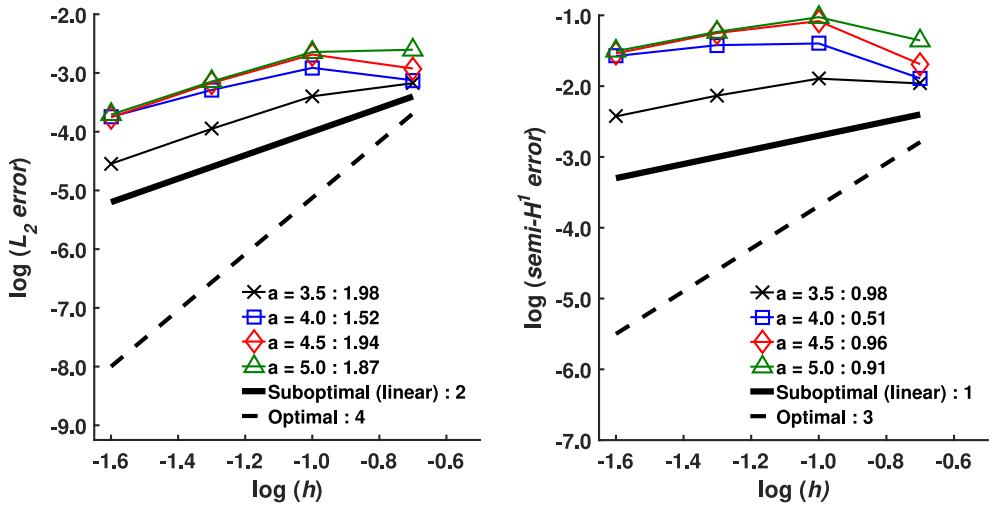

Fig. 9. Convergence of transformation method with cubic basis with various kernel measures a: rates indicated in legend.

It seems that through the popular choice of linear basis in meshfree approximations over the past two decades, this observation has somehow been overlooked, or hardly reported in the literature. To the best of the authors' knowledge, only [21] reports results with quadratic basis and strong enforcement of boundary conditions (using the RK approximation with interpolation property), where the same trend was observed.

3. Consistent weak forms for meshfree methods

3.1. Consistent weak form I: A consistent weak formulation for inadmissible test functions

A consistent weak formulation for test functions inadmissible in the conventional weak form can be derived by considering the possibility of $v^h \neq 0$ on $\partial\Omega_g$ in between nodes. First, consider the weighted residual of (8), as before:

$$(v, \nabla^2 u + s)_\Omega = 0.$$

Integrating by parts and employing divergence theorem one obtains

$$a(v,u)_\Omega = (v,s)_\Omega + (v, \boldsymbol{n}\cdot\nabla u)_{\partial\Omega}.$$

Now, by employing (8b) and allowing $v \neq 0$ on $\partial\Omega_g$, a consistent weak form which we denote ($\mathbb{W}_C^1$) is arrived at, which asks to find $u \in H_g^1$, such that for all $v \in H^1$, the following equation holds:

$$a(v,u)_\Omega - (v, \boldsymbol{n}\cdot\nabla u)_{\partial\Omega_g} = (v,s)_\Omega + (v,t)_{\partial\Omega_t} \tag{31}$$

where the requirement on $v \in H_0^1$ has been relaxed to simply $v \in H^1$ where $H^1 = H^1(\Omega)$, which allows the employment of (15) for the test function without committing a variational crime.

It is important to note, that when (31) is integrated by parts, it is straightforward to show the weak form (31) attests to (8), and the equivalence of the weak form and the strong form is verified, that is, $\mathbb{W}_C^1 \Leftrightarrow \mathbb{S}$:

$$(v, \nabla^2 u + s) + (v, h - \nabla u\cdot\boldsymbol{n})_{\partial\Omega_t}. \tag{32}$$

Since v in the above is arbitrary and $u \in H_g^1$, the strong form (8) is recovered.

The corresponding Galerkin approximation seeks $u^h \in \mathcal{S}_g$, $\mathcal{S}_g \subset H_g^1$ such that for all $v^h \in \mathcal{S}$, $\mathcal{S} \subset H^1$ the following holds

$$a(v^h,u^h)_\Omega - (v^h, \boldsymbol{n}\cdot\nabla u^h)_{\partial\Omega_g} = (v^h,s)_\Omega + (v^h,t)_{\partial\Omega_t} \tag{33}$$

where v^h is constructed from (15) and u^h is constructed from (16).

In this formulation, we have relaxed the condition on the test function, but still attempt to construct approximation spaces that satisfy the usual conditions. That is, the present weak formulation ($\mathbb{W}_C^1$) can be considered a consistent way to employ the condition $v^h = 0$ on $\partial\Omega_g$ strongly at nodes.

So far, the inconsistency in the construction of the trial function is neglected, yet in the numerical examples in Section 5 it is shown that this has little consequence on the solution accuracy. The reason for this is discussed in the Remark below.

Remark 2. Subtracting (22) from (33) gives

$$a(v^h, u^h - u)_\Omega = (v^h, \boldsymbol{n}\cdot\nabla(u^h - u))_{\partial\Omega_g} \tag{34}$$

and a type of Galerkin orthogonality is restored (compare to (23)). If one recalls that the left hand side is bounded by $a(u^h-u, u^h-u)_\Omega^{1/2}$, this indicates that the limiting term on the boundary in (23) will be released and proper convergence rates associated with the approximation space should be achieved. To emphasize, the additional term in (31) corrects for a non-zero test function on $\partial\Omega_g$, and appears to be the most important correction to the strong-type methods since it eliminates the $\mathcal{O}(h)$ term that limits the rate of convergence. The possibility that $u \neq g$ on $\partial\Omega_g$ does not seem to be as problematic, since it does not show up in (23).

Remark 3. The consistent weighted residual procedure generalizes easily to various boundary value problems (see the Appendix).

3.2. Consistent weak form II: A consistent weak formulation for inadmissible test and trial functions with symmetry

The employment of (31) yields a non-symmetric stiffness matrix which is often undesirable. In addition, unless trial functions can satisfy the essential boundary conditions exactly, we do not have $\mathbb{W}_C^1 \Leftrightarrow \mathbb{S}$, and strictly speaking $\mathbb{W}_C^1$ is still not consistent with a meshfree discretization (although as discussed previously, this may not be as problematic).

To address these two issues, consider a more general form of the weighted residual formulation with weights v_Ω on Ω and v_g on $\partial\Omega_g$:

$$(v_\Omega, \nabla^2 u + s)_\Omega + (v_g, u - g)_{\partial\Omega_g} = 0. \tag{35}$$

Various weights can be chosen, however the choice of $v_\Omega = v$ and $v_g = \boldsymbol{n}\cdot\nabla v$ yields a symmetric weak form which will be shown as follows. Further impetus is provided by the fact that a flux term $\boldsymbol{n}\cdot\nabla u$ is the "work-conjugate"

to u in terms of the potential associated with (8) and yields consistent "units" of the problem at hand. With this choice, (35) is expressed as

$$(v, \nabla^2 u + s)_\Omega + (\boldsymbol{n} \cdot \nabla v, u - g)_{\partial\Omega_g} = 0. \tag{36}$$

Integrating (36) by parts and employing the natural boundary condition (8b), one obtains a symmetric weak form that we denote $(\mathbb{W}_C^2)$, which asks to find $u \in H^1$ such that for all $v \in H^1$, the following equation holds

$$a(v, u)_\Omega - (v, \boldsymbol{n} \cdot \nabla u)_{\partial\Omega_g} - (\boldsymbol{n} \cdot \nabla v, u)_{\partial\Omega_g} = (v, s)_\Omega + (v, t)_{\partial\Omega_t} - (\boldsymbol{n} \cdot \nabla v, g)_{\partial\Omega_g}. \tag{37}$$

The above allows the complete relaxations of simply requiring $v \in H^1$ and $u \in H^1$, and now both (15) and (16) can be employed without committing a variational crime.

Applying integration by parts to $a(\cdot, \cdot)$ in (37) yields:

$$(v, \nabla^2 u + s)_{\partial\Omega} + (v, \boldsymbol{n} \cdot \nabla u - t)_{\partial\Omega_t} + (v, u - g)_{\partial\Omega_g} = 0 \tag{38}$$

where it is immediately apparent that the strong form of the problem can be recovered, hence $(\mathbb{W}_C^2) \Leftrightarrow (\mathbb{S})$.

The weak from $(\mathbb{W}_C^2)$ is the same one identified in Ref. [15], and can be also derived from a variational viewpoint. Here, the key difference between this work and that in [15], is that the weak form is employed with (15) and (16) as to rectify the deficiencies of the standard use of these approximations. We also note that employing (37) alone does not guarantee stability [16].

The corresponding Galerkin approximation seeks $u^h \in \mathcal{S}$ such that for all $v^h \in \mathcal{S}$, $\mathcal{S} \subset H^1$ the following holds

$$a(v^h, u^h)_\Omega - (v^h, \boldsymbol{n} \cdot \nabla u^h)_{\partial\Omega_g} - (\boldsymbol{n} \cdot \nabla v^h, u^h)_{\partial\Omega_g} = (v^h, s)_\Omega + (v^h, t)_{\partial\Omega_t} - (\boldsymbol{n} \cdot \nabla v^h, g)_{\partial\Omega_g} \tag{39}$$

where v^h is again constructed from (15) and u^h is constructed from (16). It is easy to see that when a Bubnov–Galerkin approximation is employed, (39) leads to a symmetric system matrix.

With the complete relaxation on test and trial functions, this weak formulation $(\mathbb{W}_C^2)$ can be considered a consistent way to employ both the conditions $v^h = 0$ on $\partial\Omega_g$ and $u^h = g$ on $\partial\Omega_g$ strongly at nodes.

Remark 4. Rather than satisfying Galerkin orthogonality, by employing (22), the Galerkin discretization of the consistent weak form $(\mathbb{W}_C^2)$ satisfies the following:

$$a\left(v^h, u^h - u\right)_\Omega = \left(\boldsymbol{n} \cdot \nabla v^h, u^h - g\right)_{\partial\Omega_g} + \left(v^h, \boldsymbol{n} \cdot \nabla(u^h - g)\right)_{\partial\Omega_g}. \tag{40}$$

Note that if $u^h = g$ on $\partial\Omega_g$, then the standard orthogonality relation is recovered.

Remark 5. The relation (40) leads to the insight that a Galerkin discretization of $(\mathbb{W}_C^2)$ minimizes the error in the norm induced by $a(\cdot, \cdot)$ augmented by the "work" of the error on the essential boundary:

$$\Pi_{(\mathbb{W}_C^2)}\left(u^h\right) = \frac{1}{2} a\left(u^h - u, u^h - u\right)_\Omega - (u^h - u, \boldsymbol{n} \cdot \nabla(u^h - u))_{\partial\Omega_g}. \tag{41}$$

That is, $(\mathbb{W}_C^2)$ can be obtained by minimization of the above potential with respect to u^h. This illuminates the possibility of balancing errors on the domain and boundary, following [29], although the numerical examples in Section 5 indicate that this is likely not necessary since optimal rates are obtained—that is, with (41), the order of errors due to the imposition of conditions on the domain and boundary may already be balanced. It should also be noted that an immediate consequence of this property is this proposed weak form also restores the ability to pass the patch test in strong-type essential boundary condition methods.

Remark 6. The potential associated with (39) can also be stated in a more conventional manner:

$$\Pi_{(\mathbb{W}_C^2)}\left(u^h\right) = \frac{1}{2} a\left(u^h, u^h\right)_\Omega - (u^h, s)_\Omega - (u^h, t)_{\partial\Omega_t} - (u^h - g, \boldsymbol{n} \cdot \nabla u^h)_{\partial\Omega_g} \tag{42}$$

where it can be seen that the last term accounts for the work done by the error on the essential boundary. Thus, considering the possibility of error on the boundary is yet another way to arrive at a consistent weak form. The other, is to minimize the error in both the domain and boundary, in terms of appropriate work-conjugates, as in (41).

Remark 7. This weak form can also be generalized to other boundary value problems, for a discussion, refer to the Appendix.

Remark 8. The employment of $(\mathbb{W}_C^2)$ or $(\mathbb{W}_C^1)$ is consistent with the variationally consistent framework proposed in [28], which requires the weak form attest to the strong form. In contrast, the strong-type of boundary condition enforcement does not. As a result a VCI method employing either of the consistent weak formulations can pass the patch test. To demonstrate this, starting from (31) or (37), and following [28], it can be shown using (8) and (4), that the requirements for obtaining an exact solution $u^{[p]}$ of order p using a *consistent* weak formulation are the same as given in [28]:

$$a\langle v^h, u^{[p]}\rangle_\Omega = -\langle v^h, \nabla^2 u^{[p]}\rangle_\Omega + \langle v^h, \boldsymbol{n}\cdot\nabla u^{[p]}\rangle_{\partial\Omega}. \tag{43}$$

Now, using integration by parts, with sufficiently high order (e.g. machine precision) quadrature one obtains:

$$a\langle v^h, u^{[p]}\rangle_\Omega \approx a(v^h, u^{[p]})_\Omega = -(v^h, \nabla^2 u^{[p]})_\Omega + (v^h, \boldsymbol{n}\cdot\nabla u^{[p]})_{\partial\Omega} \approx -\langle v^h, \nabla^2 u^{[p]}\rangle_\Omega + \langle v^h, \boldsymbol{n}\cdot\nabla u^{[p]}\rangle_{\partial\Omega} \tag{44}$$

and the pass test will be passed with higher order quadrature even if $v^h \neq 0$ on $\partial\Omega_g$ (compare to (25)). In addition, since VCI methods inherently satisfy the requirements in (43), the patch tests can be passed using (31) or (37) with any order of quadrature. This is also applicable to other variationally consistent methods such as the popular stabilized conforming nodal integration [30], or the quadratically-consistent method [31].

In summary, two weak forms have been developed, which are consistent with the inability of an approximation to meet the requirements of the conventional weak form. The first considers the fact that the weight function is possibly non-zero on the essential boundary, but that the essential boundary conditions still hold strongly. This results in a non-symmetric stiffness matrix, but is more consistent with meshfree approximations. This weak form attests to the strong form, and is shown to restore a type of Galerkin orthogonality. The second weak form relaxes the requirements on both the test and trial functions, and they only need to be constructed to possess square-integrable derivatives. The particular form taken here results in a symmetric system, at least for the model problem at hand (see the Appendix for a brief discussion). This weak form attests to the strong form, and is shown to satisfy a different orthogonality relation, which illuminates that it minimizes the error in the domain in terms of the energy norm, as well as the error on the boundary in terms of the field variable and its corresponding "flux" (or work-conjugate) term.

4. Numerical procedures

In this section, the matrix forms for the consistent weak forms are given and boundary condition enforcement procedures are discussed. As a starting point, let us first define terms common to the weak formulations discussed: let $\boldsymbol{d}$ denote a column vector of $\{u_I\}_{I\in\eta}$, Ψ_I and $\boldsymbol{B}_I$ denote the Ith shape function and the column vector of its derivatives respectively, and let $\boldsymbol{n}$ represent the unit normal to $\partial\Omega_g$ in column vector form. In two dimensions this yields:

$$\boldsymbol{d} = \begin{bmatrix} d_1 \\ d_2 \\ \vdots \\ d_{NP} \end{bmatrix}, \quad \boldsymbol{B}_I = \begin{bmatrix} \Psi_{I,1} \\ \Psi_{I,2} \end{bmatrix}, \quad \boldsymbol{n} = \begin{bmatrix} n_1 \\ n_2 \end{bmatrix}. \tag{45}$$

The following final system of matrix equations is also common to all formulations:

$$\boldsymbol{K}\boldsymbol{d} = \boldsymbol{f} \tag{46}$$

where the system size is $N_p \times N_p$. The above system is left statically uncondensed purposefully, as special procedures are needed to apply boundary conditions in meshfree methods. These techniques are discussed in Section 4.4.

4.1. Conventional weak formulation

Under the conventional weak formulation (9), the scalar entries of $\boldsymbol{K}$ and $\boldsymbol{f}$ in (46) are computed as

$$K_{IJ} = \int_\Omega \boldsymbol{B}_I^{\mathsf{T}}(\boldsymbol{x})\boldsymbol{B}_J(\boldsymbol{x})\,\mathrm{d}\Omega, \tag{47a}$$

$$f_I = \int_\Omega \Psi_I(\boldsymbol{x}) s \, \mathrm{d}\Omega + \int_{\partial\Omega_t} \Psi_I(\boldsymbol{x}) t \, \mathrm{d}\Gamma. \tag{47b}$$

4.2. Consistent weak form I (CFW I)

For the Consistent weak form I (33), the scalar entries of $\boldsymbol{K}$ and $\boldsymbol{f}$ in (46) are computed as

$$K_{IJ} = \int_\Omega \boldsymbol{B}_I^{\mathsf{T}}(\boldsymbol{x}) \boldsymbol{B}_J(\boldsymbol{x}) \, \mathrm{d}\Omega - \int_{\partial\Omega_g} \Psi_I(\boldsymbol{x}) \boldsymbol{n}^{\mathsf{T}} \boldsymbol{B}_J(\boldsymbol{x}) \, \mathrm{d}\Gamma, \tag{48a}$$

$$f_I = \int_\Omega \Psi_I(\boldsymbol{x}) s \, \mathrm{d}\Omega + \int_{\partial\Omega_t} \Psi_I(\boldsymbol{x}) t \, \mathrm{d}\Gamma. \tag{48b}$$

Comparing (48) to (47), it can be seen that only one new term is added to the stiffness matrix of the system. Later, it will be seen that the addition of this *one term* results in a drastic increase in solution accuracy and is able to restore optimal convergence rates. Indeed, the main problem with the inability to construct proper subspaces in the conventional weak formulation is due to the term in (23), which this weak form corrects for.

4.3. Consistent weak form II (CFW II)

For the discretization of consistent weak form II (39), the scalar entries of $\boldsymbol{K}$ and $\boldsymbol{f}$ in (46) are computed as

$$K_{IJ} = \int_\Omega \boldsymbol{B}_I^{\mathsf{T}}(\boldsymbol{x}) \boldsymbol{B}_J(\boldsymbol{x}) \, \mathrm{d}\Omega - \int_{\partial\Omega_g} \boldsymbol{B}_I^{\mathsf{T}}(\boldsymbol{x}) \boldsymbol{n} \, \Psi_J(\boldsymbol{x}) \, \mathrm{d}\Gamma - \int_{\partial\Omega_g} \Psi_I(\boldsymbol{x}) \boldsymbol{n}^{\mathsf{T}} \boldsymbol{B}_J(\boldsymbol{x}) \, \mathrm{d}\Gamma, \tag{49a}$$

$$f_I = \int_\Omega \Psi_I(\boldsymbol{x}) s \, \mathrm{d}\Omega + \int_{\partial\Omega_t} \Psi_I(\boldsymbol{x}) t \, \mathrm{d}\Gamma - \int_{\partial\Omega_g} \boldsymbol{B}_I^{\mathsf{T}}(\boldsymbol{x}) \boldsymbol{n} g \, \mathrm{d}\Gamma. \tag{49b}$$

In the above, it can be seen that compared to (47), both the stiffness matrix and the force vector contain new terms. For the stiffness matrix, the two additional terms are the transpose of each other, so that only one of these matrices needs to be constructed for the analysis (or just the upper triangle of the entire system matrix). In addition, since the original stiffness matrix is symmetric, the resulting system matrix will also be symmetric, and efficient solvers can be employed with this method.

4.4. Enforcement of boundary conditions

Procedurally, due to the nature of the approximations involved, it is uncommon to employ the formal definitions of test and trial approximations in (15) and (16) directly in the weak form for meshfree methods. Rather, the full systems are formed with the RK approximation defined over all nodes (1) leading to (46), and boundary conditions are applied after. That is to say, the system in (46) represents a statically uncondensed system and cannot be solved directly.

Instead, two favorable possibilities to enforce boundary conditions on the uncondensed systems are recommended here: (1) meshfree transformation procedures can be applied—the reader is referred to [17] for more details, where a simple and convenient row-swap implementation of the transformation method is presented; or (2) straightforward static condensation with direct enforcement of boundary conditions is possible (equivalent of course to using (15) and (16) directly in the weak form), provided either singular kernels [17] or shape functions with interpolation property [21] are introduced for nodes that lie on the essential boundary.

5. Numerical examples

For the following examples, the parameters of the RK approximation and the numerical integration method have been discussed in Section 2.3.4 in detail, but are briefly recalled here: twenty-by-twenty Gaussian integration per background cell is employed with cells aligned with uniformly distributed nodes. Cubic B-spline kernels are used in the RK approximation, with varying nodal spacing denoted h, kernel measures normalized with respect to h denoted a, and order of bases denoted p.

Three main methods are compared in terms of the transformation method [17]:

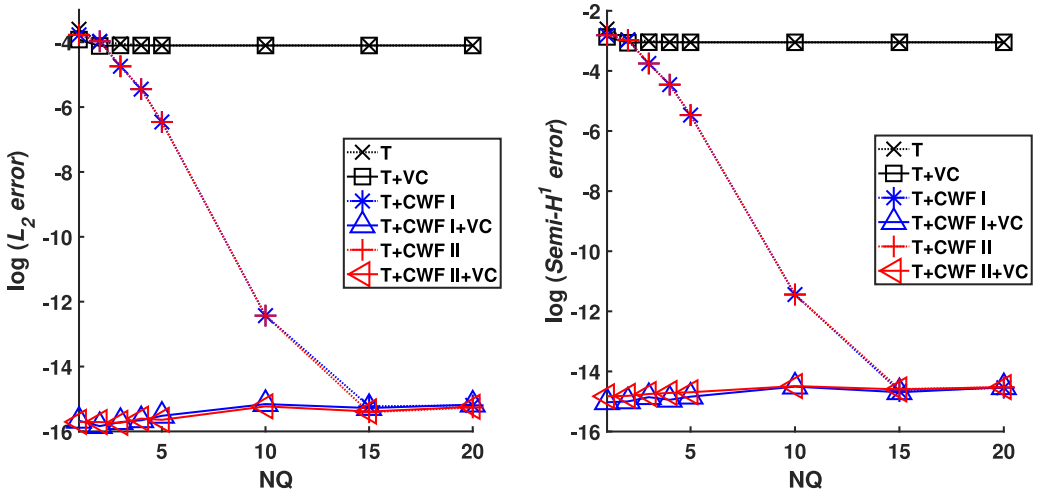

Fig. 10. Norms of error for various methods in the linear patch test. "+VC" denotes methods using VCI.

- The transformation method (denoted as T)
- The transformation method with consistent weak form I (denoted as T+CWF I)
- The transformation method with consistent weak form II (denoted as T+CWF II)

Later, the boundary singular kernel method [17] is employed to complete the study to demonstrate the method works with other types of strong enforcement, with permutations denoted following the same convention:

- The boundary singular kernel method (denoted as B)
- The boundary singular kernel method with consistent weak form I (denoted as B+CWF I)
- The boundary singular kernel method with consistent weak form II (denoted as B+CWF II)

The error in the $L_2(\Omega)$ norm and the $H^1(\Omega)$ semi-norm are assessed, computed using the same quadrature rules as forming the system matrices.

5.1. Patch test for the 2D Poisson equation

Consider the Poisson problem (8) on the domain $\bar{\Omega} = [-1, 1] \times [-1, 1]$ with the pure essential boundary condition $\partial\Omega_g = \partial\Omega$. Let the prescribed body force and boundary conditions be consistent with an exact linear solution $u = 0.1x + 0.3y$ (see (27) for the conditions).

The quadrature study in Section 2.3.4 is carried out, now with all three weak forms, to examine the effect of quadrature and use of T, T+CWF I, and T+CWF II, and VCI on the solution error in the patch test: an increasing number of quadrature points NQ is employed with these methods as before.

The error in the $L_2(\Omega)$ and $H^1(\Omega)$ semi-norm for the three versions of the transformation method are shown in Fig. 10. First, it is seen that both the proposed T+CWF I and T+CWF II are able to pass the linear patch test (with machine precision error) with sufficient quadrature. Again, the transformation method fails to pass the patch test no matter how high the order of quadrature employed.

The ability to pass the patch test by both T+CWF I and T+CWF II, and failure to pass the patch test by the transformation method alone, is consistent with the orthogonality relations (23), (34), and (40), where the resulting projection properties, or lack thereof, indicate which methods should or should not pass the patch tests. Thus the results of the patch tests are consistent with the discussions in Sections 2 and 3.

It is also seen that the variationally consistent integration technique can now pass the patch tests with any order of quadrature, provided a consistent weak form is employed (CWF I or CWF II), which is also in agreement with the discussions in Sections 2 and 3. Thus, in order to effectively use VCI to enhance solution accuracy in strong-type essential boundary condition enforcement, one must use one of the proposed consistent weak forms.

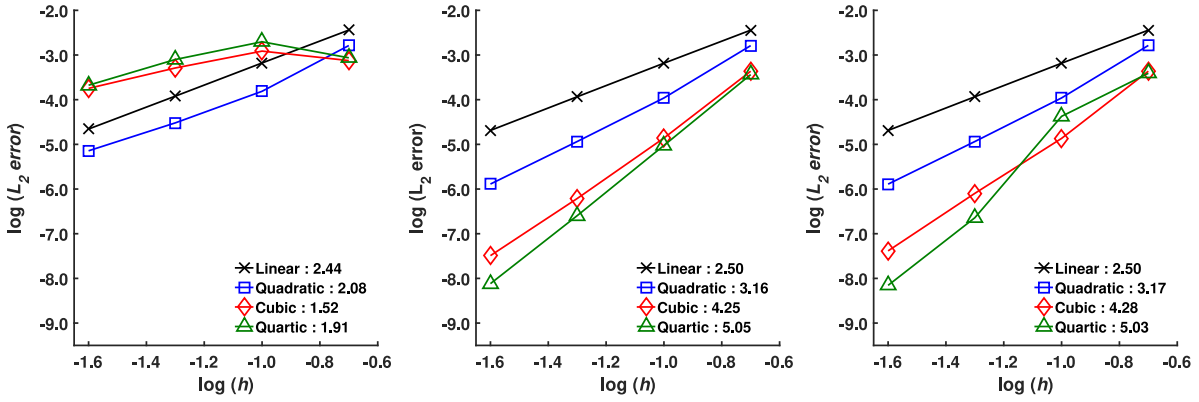

(a) T (b) T+CWF I (c) T+CWF II

Fig. 11. Convergence with various bases in the L_2 norm: rates indicated in legend.

5.2. Poisson equation with high-order solution

Now consider the Poisson problem (8), on $\bar{\Omega} = [0, 1] \times [0, 1]$, with source term and the pure essential boundary condition as the same as (29):

$$g(x, 0) = \sin(\pi x), \quad g(x, 1) = g(0, y) = g(1, y) = 0 \quad \text{on } \partial\Omega_g,$$
$$s = 0 \quad \text{in } \Omega.$$

The exact solution of this problem is high order:

$$u = \{\cosh(\pi y) - \coth(\pi)\sinh(\pi y)\}\sin(\pi x).$$

In this study, the effect of the three weak forms is examined in terms of convergence rates with respect to varying the support sizes a, order of basis functions p, and nodal spacing h. 20×20 quadrature is employed in all of the following studies in order to put aside the issue of quadrature.

5.2.1. p-refinement and h-refinement

First consider linear, quadratic, cubic, and quartic bases (denoted with $p = 1$, $p = 2$, $p = 3$, and $p = 4$, respectively), with normalized support sizes of $a = p + 1$. h-refinement is performed for each of the basis, starting with an 11×11 uniform node distribution. The solution errors in the $L_2(\Omega)$ norm and $H^1(\Omega)$ semi-norm of the various bases are plotted in Figs. 11–12, showing that T+CWF I and T+CWF II can yield optimal convergence rates ($p + 1$ in L_2 and p in semi-H^1), while the traditional weak form (T) only yields linear rates (2 in L_2 and 1 in semi-H^1), regardless of the order of basis. Therefore the present approach can yield h-refinement with pth order optimal rates of convergence.

In addition, it can be seen in Figs. 11b 11c, 12b, and 12c, that by increasing p, for any given h (with the exception of one case), more accuracy can be obtained, yielding the ability to also provide p-refinement. These two features of the present approach are in stark contrast to the results in Figs. 11a and 12a, where increasing p does not give consistently more accurate results, and in fact moving from $p = 1$ to $p = 2$ provides only marginal improvement in accuracy, while increasing p from two to three and three to four actually provides *worse results*. Comparing to Tables 1, 2, and 3, it can be inferred that this is due to the additional error in the representation of boundary conditions in the test and trial functions, decreasing from $p = 1$ to $p = 2$, and increasing from $p = 2$ to $p = 3$.

Finally, it can be noted that both T+CWF I and T+CWF II can provide p-refinement and h-refinement with pth order optimal rates with nearly the same levels of error, and one may select either based on need or preference (T+CWF I has only one new term, but yields a non-symmetric system, while T+CWF II yields a symmetric system, but has three additional terms).

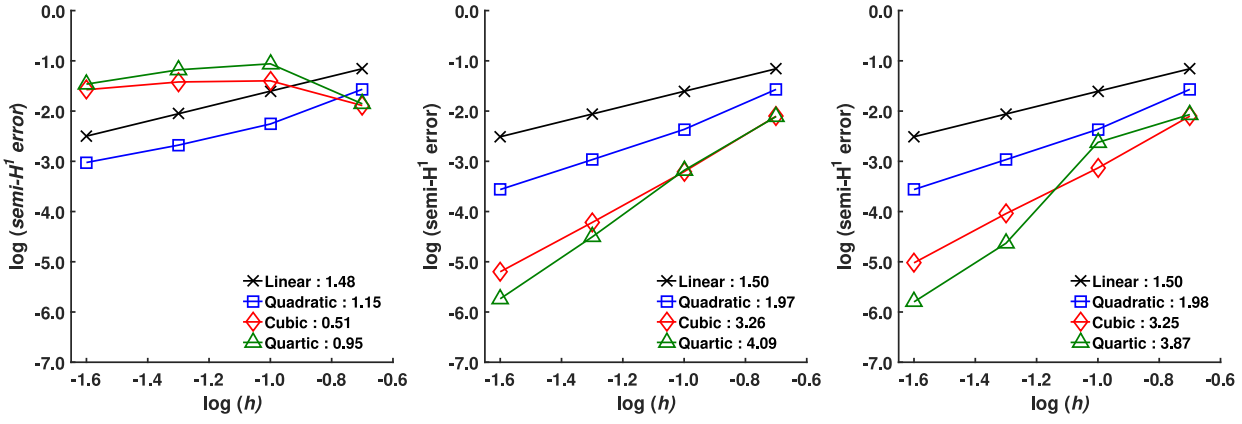

(a) T (b) T+CWF I (c) T+CWF II

Fig. 12. Convergence with various bases in the H^1 semi-norm: rates indicated in legend.

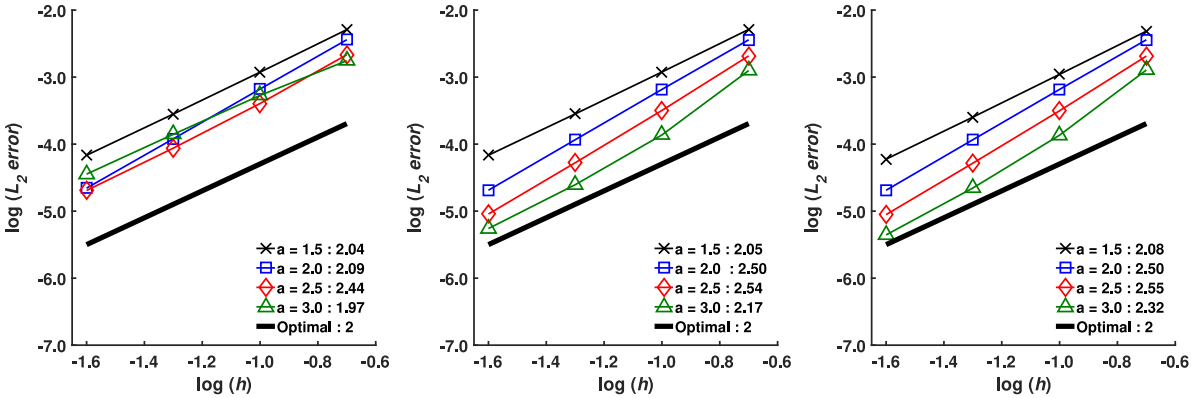

(a) T (b) T+CWF I (c) T+CWF II

Fig. 13. Convergence for linear basis ($p = 1$) with various a in the L_2 norm: rates indicated in legend.

5.2.2. Dilation analysis

The effect of varying normalized support sizes in the proposed method is now examined, since as shown previously, increased support sizes in the RK approximation can yield different behavior on the essential boundary of the domain for both test and trial functions. In addition, the present test is to show that the previous results were not a special case—window functions and their measure can have an effect on accuracy and convergence rates [26], and even super-convergence can be obtained for special values of window functions [32,33]. Thus the current permutations on a and p will examine the robustness of the formulation under the variety of free parameters in the RK approximation. For this study, the discretizations and solution technique for the previous example are employed, refining h as before, while varying a and p.

First, linear basis ($p = 1$) is tested. The errors in the $L_2(\Omega)$ norm and $H^1(\Omega)$ semi-norm are plotted in Figs. 13 and 14 respectively, for T, T+CWF I, and T+CWF II. First it can be seen that optimal rates are obtained for all cases of a, for all methods. Also, when comparing to the results for the transformation alone (T), much lower levels of error can be obtained with the present approach: nearly an order of magnitude when a is sufficiently large. The error also decreases monotonically with increasing a—this point will be revisited. Finally, it be seen that little difference in the solution error is observed for T+CWF I and T+CWF II, as in the previous cases.

Next, quadratic ($p = 2$) basis is tested for various values of a; the same error measures are presented in Figs. 15 and 16. Here it can be seen that the use of T+CWF I and T+CWF II provides a large improvement in performance over T alone, regardless of the value of a. The proposed methods provide optimal convergence rates consistently,

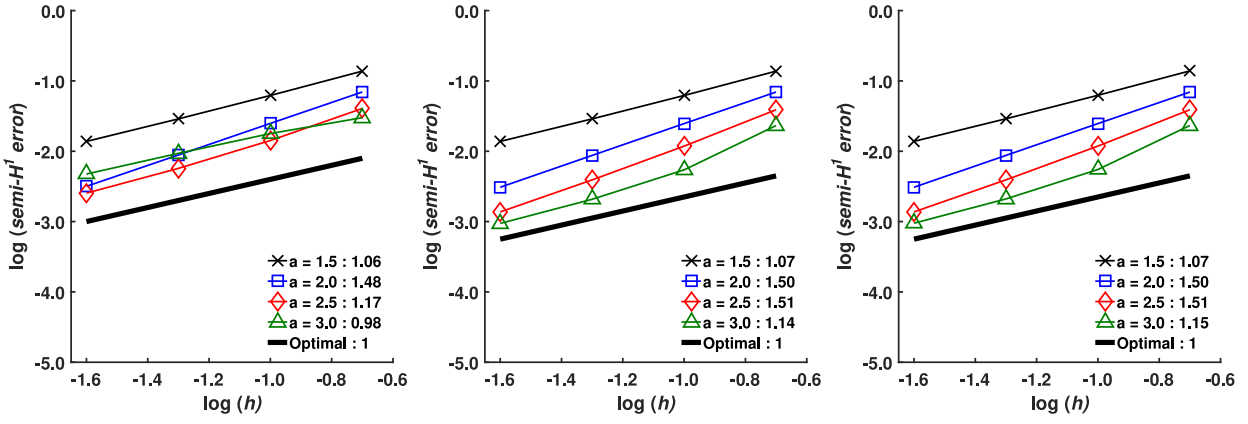

(a) T (b) T+CWF I (c) T+CWF II

Fig. 14. Convergence for linear basis ($p = 1$) with various a in the H^1 semi-norm: rates indicated in legend.

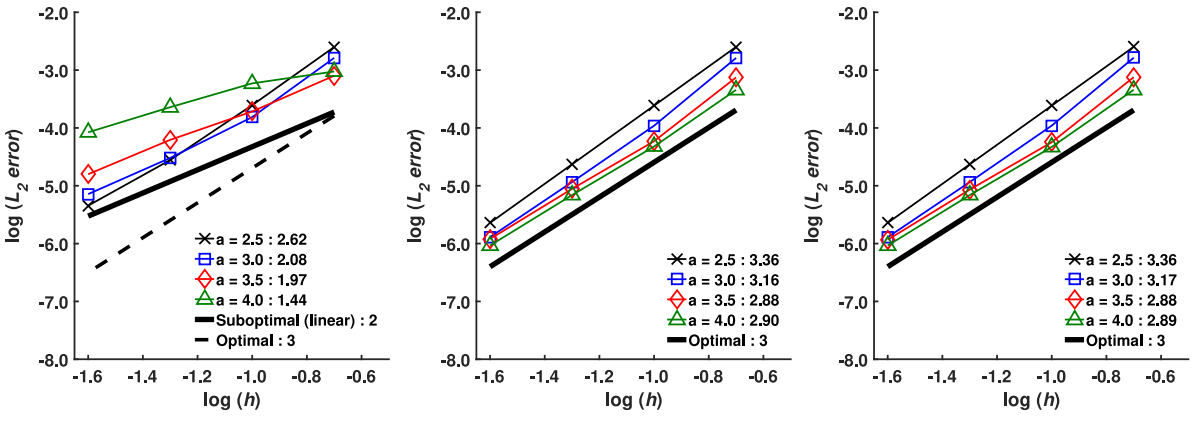

(a) T (b) T+CWF I (c) T+CWF II

Fig. 15. Convergence for quadratic basis ($p = 2$) with various a in the L_2 norm: rates indicated in legend.

and do not depend on the dilation parameter. Meanwhile, with T alone, consistently worse rates are obtained with increasing the kernel measure a. Finally, from the figures, it is starkly apparent that the magnitude of error can be reduced anywhere from one to two orders of magnitude by employing the proposed techniques.

Finally, cubic ($p = 3$) basis is tested. The same error measures are presented in Figs. 17 and 18 for all cases. Again, the two proposed methods consistently provide optimal convergence rates regardless of the value of a. However in this case, it seems that the actual value has little effect on solution accuracy. On the other hand, the transformation method (T) provides only linear rates, as expected, while the value of a also has little effect. Similar to the last example, it is apparent from Figs. 17 and 18 that these techniques provide the ability to reduce the solution error by several orders of magnitude, in this case, by three orders, or 99.9%.

5.2.3. A new concept: a-refinement

From the previous study, it can be noted that increasing the support size tends to yield lower error. This seems to run counter-intuitive as reported results in the meshfree community seem to indicate an "optimal" dilation (e.g., see [26]); this contradiction motivates the current study.

Here, a fixed distribution of the nodal spacing $h = 1/10$ is employed, while varying the normalized support a for different values of p. Fig. 19 shows the error for linear basis, where it is seen that by increasing a, lower error

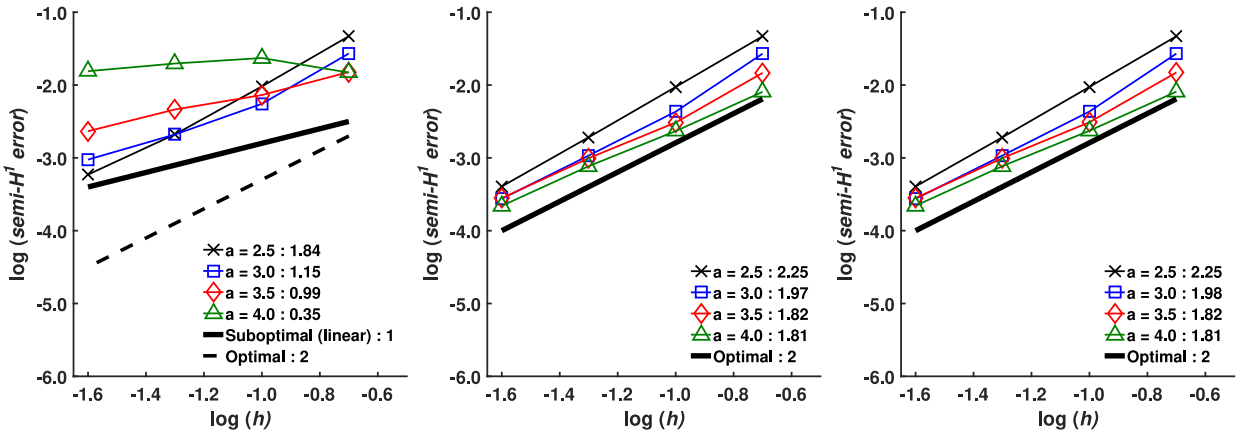

(a) T (b) T+CWF I (c) T+CWF II

Fig. 16. Convergence for quadratic basis ($p = 2$) with various a in the H^1 semi-norm: rates indicated in legend.

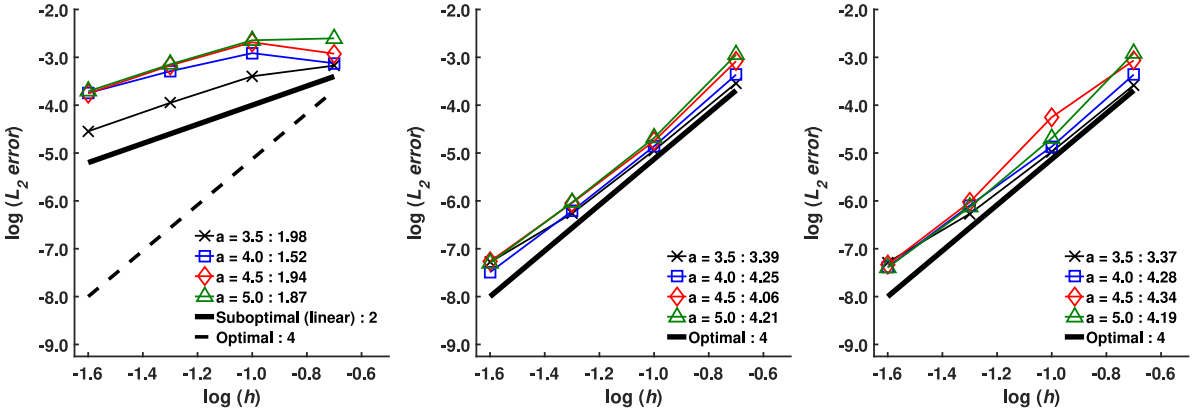

(a) T (b) T+CWF I (c) T+CWF II

Fig. 17. Convergence for cubic basis ($p = 3$) with various a in the L_2 norm: rates indicated in legend.

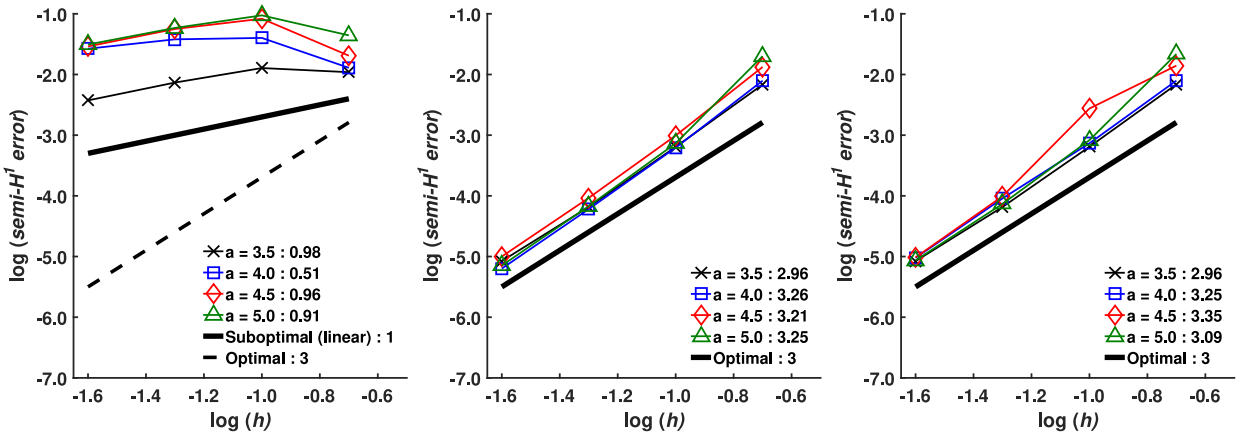

(a) T (b) T+CWF I (c) T+CWF II

Fig. 18. Convergence for cubic basis ($p = 3$) with various a in the H^1 semi-norm: rates indicated in legend.

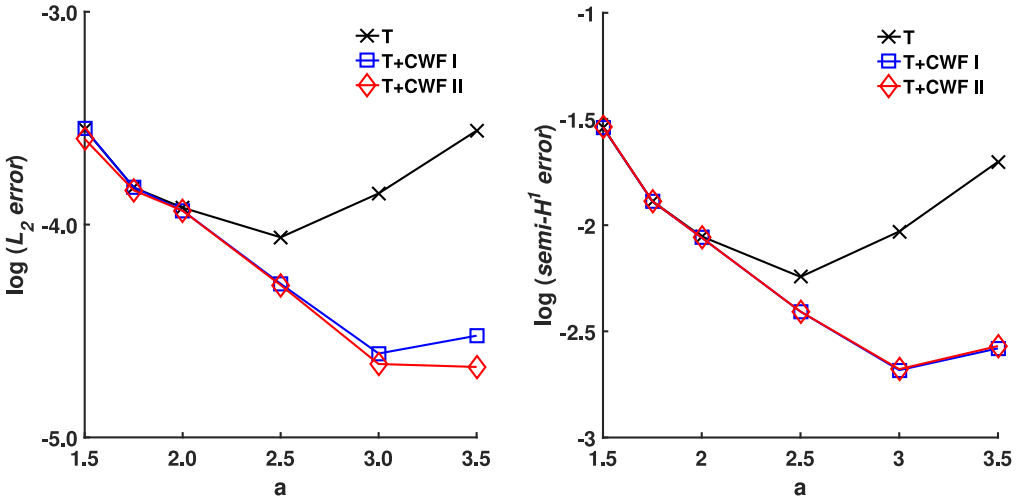

Fig. 19. Norms of error of various methods with linear basis and various kernel measures a.

can be obtained with T+CWF I and T+CWF II. On the other hand, with T alone, the optimal value appears to be $a = 2.5$, which likely strikes a balance between approximation accuracy, and error due to the inability to construct proper spaces required of the weak form.

As shown in Fig. 20, the trends are similar for quadratic basis. However this time, increasing a consistently yields larger errors for the transformation method. Meanwhile, for both T+CWF I and T+CWF II, the error is generally monotonically reduced by increasing a.

Finally, the results for cubic basis are presented in Fig. 21. Here it is seen that the kernel measure has little effect on solution accuracy, for all three methods. However for the transformation method, increasing the kernel measure monotonically increases the error. At least, the present method can obtain robust results for any selection of a in cubic basis.

To conclude, with the transformation method alone, there is an optimal value of a for linear basis. For higher-order approximations, increasing the kernel measure seems to always increase the solution error. For the proposed method, increasing a for both linear and quadratic basis very consistently yields lower error. Meanwhile, for cubic basis, the solution is relatively unaffected. In this work, we term the former effect, the ability to decrease the solution error by increasing the kernel measure, *a-refinement*. Thus with the proposed method, users may have confidence in consistent behavior of meshfree approximations in the Galerkin solution.

5.3. Boundary singular kernel method

The boundary singular kernel method is another strong type of boundary condition enforcement. Singular kernels for the reproducing kernel shape functions are introduced for essential boundary nodes, which recovers the properties (12)–(13). The imposition of boundary conditions in this method is therefore similar to the finite element method. However, since (12)–(13) do not imply the weak Kronecker delta property, values imposed may actually deviate between the nodes, just as in the transformation method.

Here we also consider the Poisson equation with high-order solution given in Section 5.2: with the boundary singular kernel method (B), boundary singular kernel method with consistent weak form one (B+CWF I), and boundary singular kernel method with consistent weak form two (B+CWF II). h-refinement is performed as before, varying p, with $a = p + 1$ fixed.

Figs. 22 and 23 show the errors in the $L_2(\Omega)$ norm and $H^1(\Omega)$ semi-norm, respectively. Here it can be seen that for B alone, the convergence rates are far from optimal, as expected from previous results and the previous discussions, and are in fact, linear. When CWFs are considered, both B+CWF I and B+CWF II can yield optimal convergence rates. That is, they allow h-refinement with pth order rates in the boundary singular kernel method. In addition, since accuracy can be increased monotonically with increasing p (again with one case as an exception), both B+CWF I and B+CWF II offer the ability to perform p-refinement.

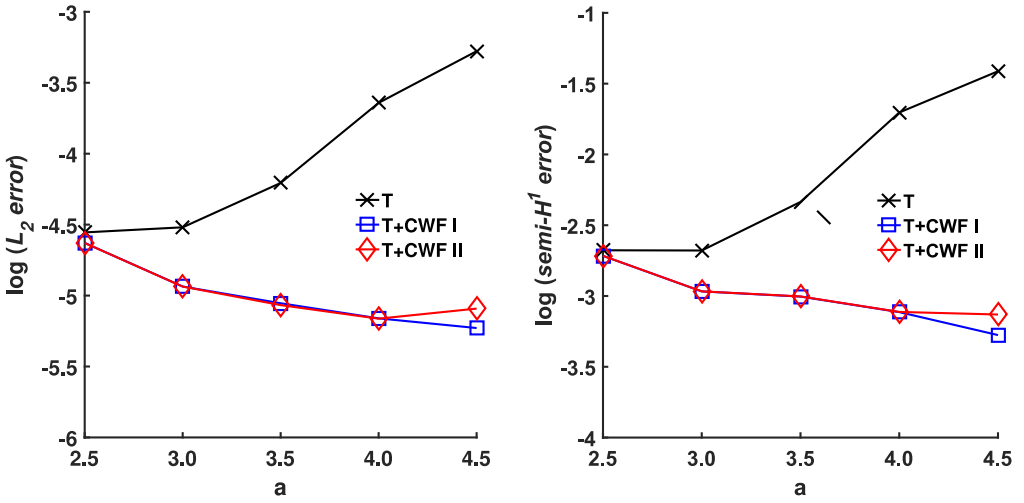

Fig. 20. Norms of error of various methods with quadratic basis and various kernel measures a.

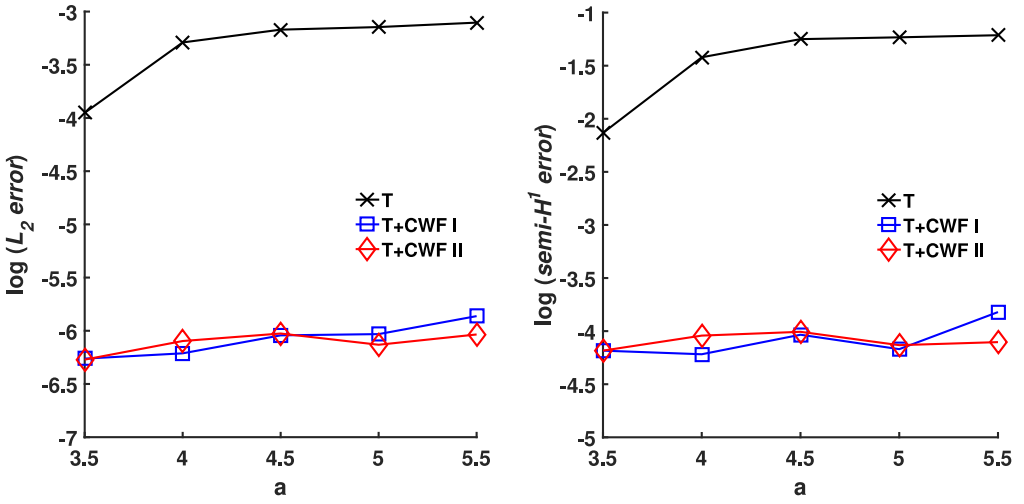

Fig. 21. Norms of error of various methods with cubic basis and various kernel measures a.

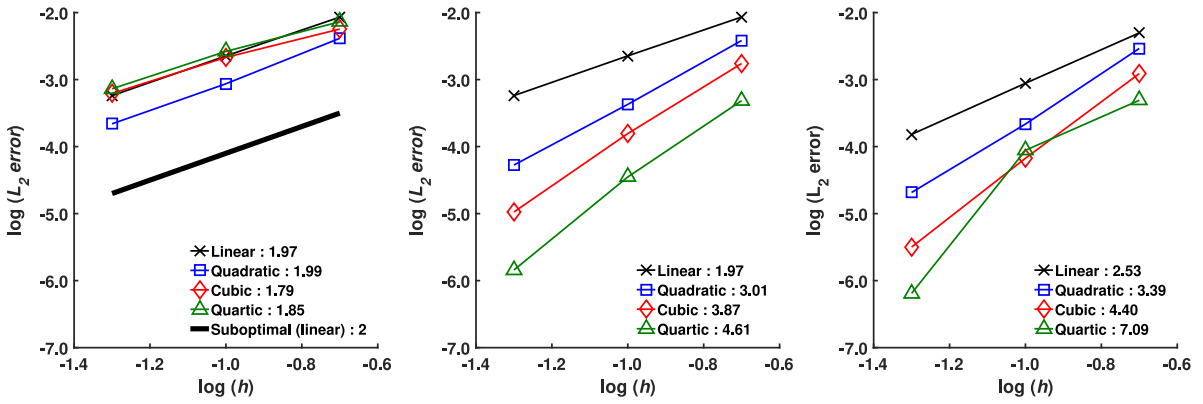

(a) B (b) B+CWF I (c) B+CWF II

Fig. 22. Convergence with various bases in the L_2 norm for the boundary singular kernel method: rates indicated in legend.

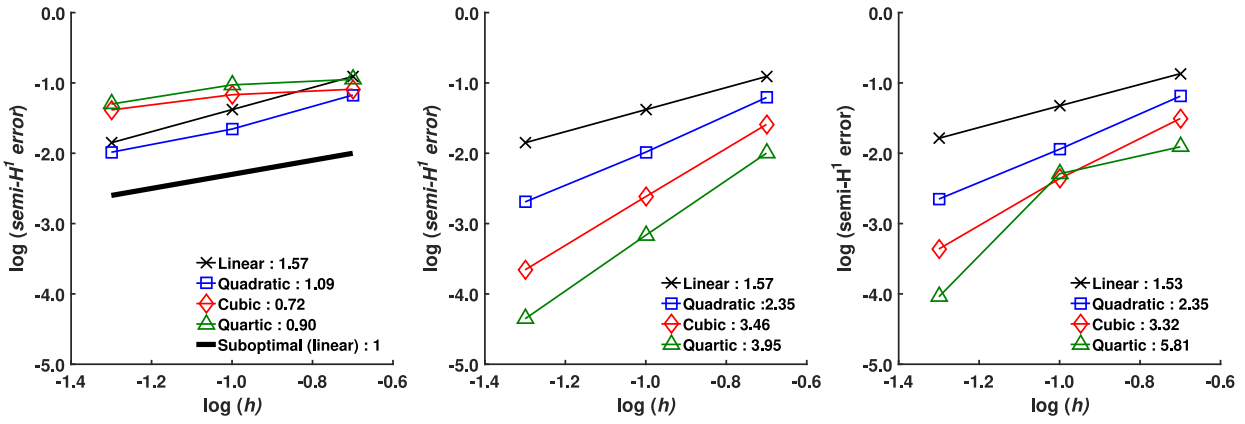

(a) B (b) B+CWF I (c) B+CWF II

Fig. 23. Convergence with various bases in the H^1 semi-norm for the boundary singular kernel method: rates indicated in legend.

6. Conclusion

In this work, it has first been shown that traditional strong enforcement of boundary conditions at nodal locations in meshfree methods is inconsistent with the traditional weak formulation of the problem. That is, without the weak Kronecker delta property, large, non-trivial deviations between the desired conditions on test and trial functions exist between nodes. This was shown to result loss of Galerkin orthogonality, and an $\mathcal{O}(h)$ error in the $L^2(\partial\Omega_g)$ norm, which in turn resulted in an $\mathcal{O}(h)$ error in the energy norm of the problem at hand. This error was also shown to be independent of the order of approximation employed. Thus, when solving PDEs, it was expected that this error would limit the rate of convergence in the numerical solution.

It was then demonstrated through patch tests, and convergence tests, that indeed this $\mathcal{O}(h)$ energy norm error appeared in the solution, limiting the rate of convergence in meshfree methods to that of linear basis. Thus, this inconsistency resulted in a barrier for meshfree approximations, to solutions with linear accuracy in the energy norm of the problem.

To remedy this deficiency, two new weak forms were introduced. The first accounts for the inconsistency in the test function construction. Here, the weak form relaxes the requirements on the test functions, to include the approximations introduced in the Galerkin equation under the strong-form enforcement framework. This weak form attests to the strong form of the problem at hand, and also was shown to restore a type of Galerkin orthogonality. Only one new term is required in the matrix formulation, however this results in a non-symmetric system matrix for self-adjoint systems.

The second weak form introduced relaxes the requirements on both the test and trial functions, to include both approximations in the strong-form enforcement methods. This weak form also attests to the strong form, and results in a symmetric system, which is favorable. Interestingly, this method results in an another orthogonality relation related to the boundary conditions, and an alternate best approximation property. The latter feature demonstrates that the method simultaneously minimizes the error in the energy norm, and the error on the boundary.

In numerical tests, it was first shown that the two proposed methods can restore the ability to pass the patch test for both high-order quadrature, and any order quadrature when VCI is employed. It was then demonstrated that pth-order optimal convergence rates under h-refinement could be obtained, which is in stark contrast to the existing strong-type methods under the conventional weak formulation. In addition, by increasing p for a fixed h, it was shown that lower error can be obtained, thus providing the ability to perform p-refinement for the first time under this framework. It was also shown that these results were independent of the particular dilation a chosen, and in fact, lower error can be obtained by increasing a, which was termed a-refinement. Taken together, the proposed method provides the ability to perform p-refinement, h-refinement with pth order rates, and a new capability called a-refinement.

Compared to other existing methods, it is apparent that the present approach is clearly superior to inconsistent strong enforcement of essential boundary conditions. In fact, this approach appears to remedy deficiencies in any

strong approach, as evidenced by the examples. Compared to weak-type methods, the present approach does not involve tunable parameters, nor does it involve additional degrees of freedom or stability conditions. However, since the present approach includes Nitsche-type terms, it is possible that with the proper selection of the penalty parameter in Nitsche's approach, it would be less efficient. However, by comparison, the present approach does not require computation or user selection of any parameters, and can still ensure optimal convergence.

Finally, it should be noted that in this work, high-order quadrature was employed, which is atypical of a practical meshfree implementation. In future work, this aspect should be investigated: for instance, what is the lowest order quadrature required to maintain these high-order properties? And, with methods such as variationally consistent integration, which can greatly reduce the burden of quadrature, what would be the order required? It is noteworthy that the present technique is compatible with the variationally consistent approach, in that the weak forms attest to the strong form of the problem, which is in contrast to traditional strong enforcement of boundary conditions. Lastly, this method was tested for the Poisson equation, but can be applied to other boundary value problems as well, as described in the Appendix.

Acknowledgments

The authors greatly acknowledge the support of this work by the L. Robert and Mary L. Kimball Early Career Professorship.

Declaration of competing interest

The authors declare that they have no known competing financial interests or personal relationships that could have appeared to influence the work reported in this paper.

Appendix

Consider the following abstract boundary value problem governing a scalar u:

$$Lu + s = 0 \quad \text{in } \Omega \tag{51a}$$

$$Bu = t \quad \text{on } \partial\Omega_t \tag{51b}$$

$$u = g \quad \text{on } \partial\Omega_g \tag{51c}$$

where L is scalar differential operator acting in the domain $\Omega \subset \mathbb{R}^d$, s is a source term, B is a scalar boundary operator acting on the natural boundary $\partial\Omega_t$, t is the prescribed values of Bu on $\partial\Omega_t$, g is the prescribed values of u on the essential boundary $\partial\Omega_g$, $\partial\Omega_g \cap \partial\Omega_t = \emptyset$ and $\partial\Omega = \overline{\partial\Omega_g \cup \partial\Omega_t}$.

Consider the weighted residual of the boundary value problem:

$$(v, Lu + s)_\Omega = 0. \tag{52}$$

Manipulation yields a bilinear form $a(\cdot,\cdot)$ which results from the integration by parts formula $(v, Lu)_\Omega = (v, Bu)_{\partial\Omega} - a(v, u)_\Omega$, and the following problem statement for $(\mathbb{W}_C^1)$: find $u \in H_g^k$, $H_g^k = \{u | u \in H^k(\Omega), u = g \text{ on } \partial\Omega_g\}$ such that for all $v \in H^k$ the following equation holds:

$$a(v, u)_\Omega - (v, Bu)_{\partial\Omega_g} = (v, s)_\Omega + (v, t)_{\partial\Omega_t} \tag{53}$$

where H^k is an adequate Sobolev space. The above is a consistent weighted residual of the boundary value problem as $v = 0$ on $\partial\Omega_g$ is not required to verify it. Note that this procedure does not require the governing equation to emanate from a potential.

To take a concrete example, consider the equations for elasticity:

$$\nabla \cdot \boldsymbol{\sigma} + \boldsymbol{b} = \boldsymbol{0} \quad \text{in } \Omega \tag{54a}$$

$$\boldsymbol{\sigma} \cdot \boldsymbol{n} = \boldsymbol{t} \quad \text{on } \partial\partial\Omega_t \tag{54b}$$

$$\boldsymbol{u} = \boldsymbol{g} \quad \text{on } \partial\Omega_{\boldsymbol{g}} \tag{54c}$$

where $\boldsymbol{u}$ is the displacement, $\boldsymbol{b}$ is the body force, $\boldsymbol{t}$ is the traction, $\boldsymbol{g}$ is the prescribed displacement, $\boldsymbol{n}$ is the unit normal to the domain, $\boldsymbol{\sigma} = \mathbb{C} : \nabla^s \boldsymbol{u}$ is the Cauchy stress tensor; $\mathbb{C}$ is the elasticity tensor and $\nabla^s \boldsymbol{u} = 1/2(\nabla \otimes \boldsymbol{u} + \boldsymbol{u} \otimes \nabla)$ is the strain tensor.

The following form for $(\mathbb{W}_C^1)$ can be obtained following the given procedures: find $\boldsymbol{u} \in \mathcal{S}_g$, $\mathcal{S}_g = \{\boldsymbol{u} | \boldsymbol{u} \in H^1(\Omega), u_i = g_i \text{ on } \partial\Omega_{g_i}\}$ such that for all $\boldsymbol{w} \in H^1$ the following equation holds:

$$a(\boldsymbol{w}, \boldsymbol{u})_\Omega - (\boldsymbol{w}, \boldsymbol{n} \cdot \sigma(\boldsymbol{u}))_{\partial\Omega_{\boldsymbol{g}}} = (\boldsymbol{w}, \boldsymbol{b})_\Omega + (\boldsymbol{w}, \boldsymbol{t})_{\partial\Omega_{\boldsymbol{t}}} \tag{55}$$

where

$$a(\boldsymbol{w}, \boldsymbol{u})_\Omega = \int_\Omega \nabla^{\mathrm{s}} \boldsymbol{w} : \mathbb{C} : \nabla^{\mathrm{s}} \boldsymbol{u} \, \mathrm{d}\Omega, \tag{56a}$$

$$(\boldsymbol{w}, \boldsymbol{b})_\Omega = \int_\Omega \boldsymbol{w} \cdot \boldsymbol{b} \, \mathrm{d}\Omega, \tag{56b}$$

$$(\boldsymbol{w}, \boldsymbol{t})_{\partial\Omega_{\boldsymbol{t}}} = \int_{\partial\Omega_{\boldsymbol{t}}} \boldsymbol{w} \cdot \boldsymbol{t} \, \mathrm{d}\Gamma, \tag{56c}$$

$$(\boldsymbol{w}, \boldsymbol{n} \cdot \sigma(\boldsymbol{u}))_{\partial\Omega_{\boldsymbol{g}}} = \int_{\partial\Omega_{\boldsymbol{g}}} \boldsymbol{w} \cdot (\boldsymbol{n} \cdot \sigma(\boldsymbol{u})) \, \mathrm{d}\Gamma. \tag{56d}$$

For the symmetric weak form of the abstract scalar boundary value problem, consider a more general weighted residual:

$$(v_\Omega, Lu + s)_\Omega + \left(v_g, u - g\right)_{\partial\Omega_g} = 0. \tag{57}$$

Choosing $v_\Omega = v$ and $v_g = Bv$ one obtains the following formulation for $(\mathbb{W}_C^2)$: find $u \in H^k$ such that for all $v \in H^k$ the following equation holds

$$a(v, u)_\Omega - (v, Bu)_{\partial\Omega_g} - (Bv, u)_{\partial\Omega_g} = (w, s)_\Omega + (v, t)_{\partial\Omega_t} - (Bv, g)_{\partial\Omega_g} \tag{58}$$

where H^k is again an adequate Sobolev space. The above verifies the boundary value problem without the use of $v = 0$ on $\partial\Omega_g$ and $u = g$ on $\partial\Omega_g$. Note that if L is non-self-adjoint $a(\cdot, \cdot)$ is not symmetric, and the resulting Galerkin system matrix will not be symmetric.

To take an example, consider the elasticity equations again. The $(\mathbb{W}_C^2)$ can be derived as: find $\boldsymbol{u} \in H^1$, such that for all $\boldsymbol{w} \in H^1$ the following equation holds:

$$a\left(\boldsymbol{w}, \boldsymbol{u}\right)_\Omega - (\boldsymbol{w}, \boldsymbol{\sigma}\left(\boldsymbol{u}\right) \cdot \boldsymbol{n})_{\partial\Omega_{\boldsymbol{g}}} - (\boldsymbol{\sigma}\left(\boldsymbol{w}\right) \cdot \boldsymbol{n}, \boldsymbol{u})_{\partial\Omega_{\boldsymbol{g}}} = (\boldsymbol{w}, \boldsymbol{b})_\Omega + (\boldsymbol{w}, \boldsymbol{h})_{\partial\Omega_h} - (\boldsymbol{\sigma}\left(\boldsymbol{w}\right) \cdot \boldsymbol{n}, \boldsymbol{g})_{\partial\Omega_{\boldsymbol{g}}}. \tag{59}$$

Again, this procedure does not require the governing equation to emanate from a potential, although from the discussions in the manuscript, it seems that this is likely always possible to do so if the original governing equation does.

References

[1] J.-S. Chen, M. Hillman, S.-W. Chi, Meshfree methods: Progress made after 20 years, J. Eng. Mech. 143 (4) (2016) 04017001.

[2] T. Belytschko, Y. Krongauz, D. Organ, M. Fleming, P. Krysl, Meshless methods: An overview and recent developments, Comput. Methods Appl. Mech. Engrg. 139 (1–4) (1996) 3–47.

[3] S. Li, W.K. Liu, Meshfree and particle methods and their applications, Appl. Mech. Rev. 55 (1) (2002) 1–34.

[4] J.-S. Chen, S.-W. Chi, H.-Y. Hu, Recent developments in stabilized Galerkin and collocation meshfree methods, Comput. Assist. Methods Eng. Sci. 18 (1/2) (2017) 3–21.

[5] J.-S. Chen, C. Pan, C.-T. Wu, W.K. Liu, Reproducing kernel particle methods for large deformation analysis of non-linear structures, Comput. Methods Appl. Mech. Engrg. 139 (1–4) (1996) 195–227.

[6] Y.X. Mukherjee, S. Mukherjee, On boundary conditions in the element-free Galerkin method, Comput. Mech. 19 (4) (1997) 264–270.

[7] T.L. Zhu, S.N. Atluri, A modified collocation method and a penalty formulation for enforcing the essential boundary conditions in the element free Galerkin method, Comput. Mech. 21 (3) (1998) 211–222.

[8] S.N. Atluri, J.Y. Cho, H.G. Kim, Analysis of thin beams, using the meshless local Petrov–Galerkin method, with generalized moving least squares interpolations, Comput. Mech. 24 (5) (1999) 334–347.

[9] G.J. Wagner, W.K. Liu, Application of essential boundary conditions in mesh-free methods: A corrected collocation method, Internat. J. Numer. Methods Engrg. 47 (8) (2000) 1367–1379.

[10] T. Belytschko, Y.Y. Lu, L. Gu, Element-free Galerkin methods, Internat. J. Numer. Methods Engrg. 37 (2) (1994) 229–256.

[11] J. Nitsche, Über ein Variationsprinzip zur Lösung von Dirichlet-Problemen bei Verwendung von Teilräumen, die keinen Randbedingungen unterworfen sind, Abh. Math. Semin. Univ. Hambg. 36 (1) (1971) 9–15.

[12] S. Fernández-Méndez, A. Huerta, Imposing essential boundary conditions in mesh-free methods, Comput. Methods Appl. Mech. Engrg. 193 (12) (2004) 1257–1275.

[13] I. Babuška, The finite element method with Lagrangian multipliers, Numer. Math. 20 (3) (1973) 179–192.

[14] F. Brezzi, On the existence, uniqueness and approximation of saddle-point problems arising from Lagrangian multipliers, Publ. Math. Inform. Rennes (S4) (1974) 1–26.
[15] Y.Y. Lu, T. Belytschko, L. Gu, A new implementation of the element free Galerkin method, Comput. Methods Appl. Mech. Engrg. 113 (3–4) (1994) 397–414.
[16] M. Griebel, M.A. Schweitzer, A particle-partition of unity method part V: boundary conditions, in: Geometric Analysis and Nonlinear Partial Differential Equations, Springer, Berlin, Heidelberg, 2003, pp. 519–542.
[17] J.-S. Chen, H.-P. Wang, New boundary condition treatments in meshfree computation of contact problems, Comput. Methods Appl. Mech. Engrg. 187 (3–4) (2000) 441–468.
[18] T. Belytschko, D. Organ, Y. Krongauz, A coupled finite element-element-free Galerkin method, Comput. Mech. 17 (3) (1995) 186–195.
[19] Y. Krongauz, T. Belytschko, Enforcement of essential boundary conditions in meshless approximations using finite elements, Comput. Methods Appl. Mech. Engrg. 131 (1–2) (1996) 133–145.
[20] L.T. Zhang, G.J. Wagner, W.K. Liu, A parallelized meshfree method with boundary enrichment for large-scale CFD, J. Comput. Phys. 176 (2) (2002) 483–506.
[21] J.-S. Chen, W. Han, Y. You, X. Meng, A reproducing kernel method with nodal interpolation property, Internat. J. Numer. Methods Engrg. 56 (7) (2003) 935–960.
[22] J. Gosz, W.K. Liu, Admissible approximations for essential boundary conditions in the reproducing kernel particle method, Comput. Mech. 19 (1) (1996) 120–135.
[23] B. Nayroles, G. Touzot, P. Villon, Generalizing the finite element method: Diffuse approximation and diffuse elements, Comput. Mech. 10 (5) (1992) 307–318.
[24] J.J. Koester, J.-S. Chen, Conforming window functions for meshfree methods, Comput. Methods Appl. Mech. Engrg. 347 (2019) 588–621.
[25] F.C. Günther, W.K. Liu, Implementation of boundary conditions for meshless methods, Comput. Methods Appl. Mech. Engrg. 163 (1–4) (1998) 205–230.
[26] W.K. Liu, S. Jun, Y.F. Zhang, Reproducing kernel particle methods, Internat. J. Numer. Methods Fluids 20 (8–9) (1995) 1081–1106.
[27] G.J. Strang, Gilbert, Fix, An Analysis of the Finite Element Method, Prentice-hall, Englewood Cliffs, NJ, 1973.
[28] J.-S. Chen, M. Hillman, M. Rüter, An arbitrary order variationally consistent integration for Galerkin meshfree methods, Internat. J. Numer. Methods Engrg. 95 (5) (2013) 387–418.
[29] H.Y. Hu, J.S. Chen, W. Hu, Weighted radial basis collocation method for boundary value problems, Internat. J. Numer. Methods Engrg. 69 (13) (2007) 2736–2757.
[30] J.-S. Chen, C.-T. Wu, S. Yoon, Y. You, A stabilized conforming nodal integration for Galerkin mesh-free methods, Internat. J. Numer. Methods Engrg. 50 (2) (2001) 435–466.
[31] Q. Duan, X. Li, H. Zhang, T. Belytschko, Second-order accurate derivatives and integration schemes for meshfree methods, Internat. J. Numer. Methods Engrg. 92 (4) (2012) 399–424.
[32] S. Li, W.K. Liu, Moving least-square reproducing kernel method part ii: Fourier analysis, Comput. Methods Appl. Mech. Engrg. 139 (1–4) (1996) 159–193.
[33] Y. Leng, X. Tian, J.T. Foster, Super-convergence of reproducing kernel approximation, Comput. Methods Appl. Mech. Engrg. 352 (2019) 488–507.